UNIVERSIDADE D
COIMBRA

PIAL DAS

# TRIBOLOGICAL PERFORMANCE OF CARBON ALLOYED TRANSITION METAL DICHALCOGENIDE COATINGS IN NITRILE BUTADIENE RUBBER CONTACTS

**VOLUME 1**

**Dissertação no âmbito do Mestrado Conjunto Europeu em Tribologia de Superfícies e Interfaces orientada pelos Dr. Albano Cavaleiro e Dr. Todor Vuchkov e apresentada ao Departamento de Engenharia Mecânica da Faculdade de Ciências e Tecnologia da Universidade de Coimbra.**

Julho de 2022

1 2 9 0

FACULDADE DE CIÊNCIAS E TECNOLOGIA
UNIVERSIDADE D COIMBRA

# Tribological performance of carbon alloyed transition metal dichalcogenide coatings in nitrile butadiene rubber contacts

Submitted in Partial Fulfilment of the Requirements for the Degree of European Joint European Master in Tribology of Surfaces and Interfaces.

# Desempenho tribológico de revestimentos de dicalcogenetos de metais de transição dopados com carbono em contacto com borracha nitrilo-butadieno


**Author**

**Pial Das**

**Advisor[s]**

**Dr. Albano Cavaleiro**

**Dr. Todor Vuchkov**


**Jury**

| | |
|---|---|
| **President** | **Professor Doutor Bruno Trindade**<br>**Professor at University of Coimbra** |
| **Vowel** | **Professor Doutor Ricardo Serra**<br>**Professor at University of Coimbra** |
| **Advisor(s)** | **Professor Doutor Albano Cavaleiro**<br>**Professor at University of Coimbra**<br>**Doutor Todor Vuchkov**<br>**Researcher at Instituto Pedro Nunes** |

1 2 9 0

UNIVERSIDADE D COIMBRA

**COIMBRA, JULY, 22**

tribos

# ACKNOWLEDGEMENTS

I would like to express my gratitude to all who have contributed to completing the project described in this thesis.

First and foremost, I would like to thank my advisors, Dr. Albano Cavaleiro and Dr. Todor Vuchkov from the University of Coimbra and IPN respectively, for their guidance and valuable input during the project.

Special thanks to the TRIBOS consortium for providing me with this life-changing opportunity and the European Commission's funding. I wish well for my TRIBOS mentors Professor Ardian Morina, Professor Mitjan Kalin, and Professor Bruno Trindade for, their support.

Finally, I want to express my profound gratitude to my parents, family, and friends who have offered constant support and encouragement, directly or indirectly, throughout this degree and while writing this thesis.

# Abstract

In recent years some of the promising applications of solid lubricants in diverse environments have caught a lot of attention. In this regard, a transition metal dichalcogenide (TMD) could provide some favorable solutions due to its highly anisotropic multilayered structure. However, the pure TMD has some inherent drawbacks, which could be optimized by introducing doping elements of different metal compounds and nonmetal atoms. In this study, a quite familiar TMD, tungsten disulfide ($WS_2$), has been alloyed with carbon (C) to improve its mechanical and failure properties while preserving its main attribute of low friction properties to a favorable level. Four different TMD coatings have been deposited in a semi-industrial-sized closed field unbalanced magnetron sputtering deposition machine, which allowed us to have better control on the composition and uniformity of the obtained coatings. Tribological and mechanical characterization of the coatings has been performed. The morphology and crystallinity have been studied. The use of substrate bias in the unalloyed coatings during deposition resulted in their improved performance in terms of failure and hardness, the latter of which has been further extended by the additional percentage of C in the coatings. The effect of temperature has also been investigated and it has been found that at a higher temperature both the unalloyed and alloyed coatings perform better in terms of coefficient of friction. The nanocrystalline $WS_2$ phase has been found responsible for the low friction properties of all of sulfur sub-stoichiometric coatings analyzed in this study. S/W ratio has been found to play an important role to improve frictional properties, yet diminishing the mechanical and failure properties.



*Keywords*: TMDs, WSC films, Structure, Mechanical and Tribological properties

# Resumo

Nos últimos anos, algumas das aplicações mais promissoras dos lubrificantes sólidos em diversos ambientes despertaram muita atenção. A este respeito, o dicalcogeneto de metal de transição (TMD) pode fornecer algumas soluções favoráveis devido à sua estrutura multicamada altamente anisotrópica. Ainda assim, o TMD puro tem algumas desvantagens inerentes, que poderiam ser otimizadas através da introdução de elementos dopantes, sob a forma de diferentes compostos metálicos ou atómos não metálicos. Neste estudo, um TMD bastante familiar, dissulfeto de tungstênio ($WS_2$), foi dopado com C tendo em vista a melhoria das suas propriedades mecânicas e de comportamento à falha e a simultânea preservação das suas propriedades de baixo atrito a um nível favorável, aquele que é considerado o seu maior atributo. Quatro revestimentos TMD diferentes foram depositados numa máquina de deposição de magnetrão não balanceado de campo próximo de tamanho semi-industrial, a qual nos permitiu deter um maior controlo sobre a composição e uniformidade dos revestimentos obtidos. A caracterização tribológica e mecânica dos revestimentos foi realizada. A morfologia e a cristalinidade foram estudadas. O uso de polarização do substrato nos revestimentos não ligados durante a sua deposição resultou no seu melhor desempenho em termos de comportamento à falha e de dureza, sendo que a última foi adicionalmente estendida pelo aumento da percentagem de C nos revestimentos. O efeito da temperatura também foi investigado e verificou-se que a uma temperatura mais elevada tanto os revestimentos não ligados como os ligados têm melhor desempenho no que diz respeito ao seu coeficiente de atrito. A fase nanocristalina $WS_2$ foi considerada responsável pelas propriedades de baixo atrito de todos os revestimentos subestequiométricos de enxofre analisados neste estudo. Verificou-se que o rácio S/W desempenha um papel importante na melhoria das propriedades de fricção dos revestimentos, ainda que piore as suas propriedades mecânicas e o comportamento à falha.

*Palavras-chave*: TMDs, filmes WSC, Estrutura, Propriedades Mecânicas e Tribológicas

# [LIST OF FIGURES]

# [LIST OF TABLES]



# [LIST OF SIMBOLS] AND [ACRONYMS/ ABBREVIATIONS

## [List of Symbols]

℃– Degrees Celcius

~ – Approximately

E – Reduced Elastic Modulus

H – Hydrogen

C – Carbon

N – Nitrogen

O – Oxygen

Ar – Argon

## [Acronyms/Abbreviations]

TMD – Transition metal dichalcogenide

NBR – Nitrile butadiene rubber

PVD – Physical vapour deposition

CVD – Chemical vapour deposition

SWR – Specifiq wear rate

ASTM – American Society for Testing and Materials

AISI – American Iron and Steel Institute

UV – Ultra Violate

DC – Direct Current

$MoS_2$ – Molybdenum disulphide

$WS_2$ – Tungsten disulphide

TMD-C – Carbon doped transition metal dichalcogenide

DLC – Diamond like carbon coatings

$H_2$ – Hydrogen gas

$N_2$ – Nitrogen gas

CFUMS – Close Field Unballence Magnitron Sputtering

$CO_2$ – Carbon dioxide

TiC – Titanium carbide

CrN – Chromium nitride

WC – Tungsten carbide

TiAlN – Titanium aluminum nitride

TMD-C – Carbon doped transition metal dichalcogenide

FCTUC – Faculdade de Ciências e Tecnologia da Universidade de Coimbra

DEM – Departamento de Engenharia Mecânica

# CONTENTS

# CHAPTER 1

## 1. Introduction

Friction is arguably the most known phenomenon in the field of mechanical engineering. It is created by forces acting on the surfaces of interacting entities at their interface. The amount of these frictional forces is determined by the qualities of the two contacting surfaces as well as the properties of the two materials. As the surface qualities may vary over time due to deformation, wear, component segregation, and oxidation, these forces are frequently difficult to forecast. Additionally, due to the roughness of the contact surfaces, the effective contact area between the bodies differs from the apparent surface area of the bodies [1].

Although sometimes friction is desirable (in the absence of friction we can't even walk), most of the time it creates problems such as the additional need for energy, thermal degradation, and wear. Every year, around 100 million terajoules of energy are needed to overcome friction across the world, accounting for nearly one-fifth of all energy generated. The industry and transportation sectors contribute a large percentage of total energy consumed to overcome friction, almost 29%, and 30% respectively. According to recent studies on energy usage in passenger vehicles, trucks, and buses, it is possible to save up to 17.5 % of the energy used in road transportation in the short term (5 - 9 years) by implementing innovative tribological solutions effectively. This translates into yearly energy savings of 11.6 exajoules, or fuel savings of 330 billion liters and an 860 million tons decrease in $CO_2$ emissions[2]. So, it is possible to reduce a huge amount of carbon footprint from the industry just by reducing the associated friction.

To mitigate the problem of friction generally liquid (oil) or semi-liquid (grease) lubrication is used. Although the classical oil lubrication system provides reduced friction, reduction of wear, protection of the equipment from corrosion, control of temperature (heat dissipation), control of contamination (by removing it from the system), the transmission of power (hydraulics), fluid sealing, sometimes their environmental impact could be questionable for the new generation of design and manufacturing engineers. In some specific engineering applications, classical lubrication is not even applicable and the self-lubrication properties of materials can come in handy, for example, lubrication in the vacuum environment, elevated temperature, and

equipment sealed for life scenarios. Although typical self-lubricant solid materials cannot provide structural strength for most applications, their layers of coating on the core structural material could be considered an innovative technique. Since wear and friction are surface phenomena, a component's tribological performance can be improved by properly designing the surface. Generally, the coating is often just a few micrometers thick, or a few thousandths of a millimeter. Even so, it may significantly reduce friction and wear. Coatings generally utilize the advantages of tribo-active films, which are slightly different from the bulk coating. The outermost surface which actually comes into contact with the sliding body creates this film, just a few tens of nanometers thick, which contributes significantly to the coating performance. Tribo-active coatings can be defined as the coatings that spontaneously form and sustain tribo-film at the desired property[3], which recently has become quite a point of attention for the scientific community.

The procedure of using friction reduction coatings can also be employed in the polymer molding industries where one of the most significant drawbacks is that the finished products frequently adhere to the mold, especially in tire manufacturing industries. Mold fouling is a related issue in which deposits from prior production adhere to the surface of the mold, resulting in defects in the following production unit. Mold release and mold fouling have important ramifications for the polymer sector in terms of reducing production rate, which may be a considerable expense in the industry[4]. There are some chemical agents available commercially for the polymer industries to mitigate this problem, but their use can affect the quality of the finished product and can also be time-consuming, providing no effective solution to this problem[5]. The entire process of rubber molding may be perceived as a simple metallic surface in rubber contact, pushing the motivation of investigating the tribological behavior of TMD coatings against nitrile butadiene rubber (NBR), giving the goal of this study to explore the tribological behavior of TMD coating in rubber contact.

In this experimental study physical vapor deposition technique (PVD) has been used to deposit TMD coatings. A reciprocating ball-on-disc tribometer will be used for tribological characterization. The behavior of TMD coatings in rubber contact will next be studied using a variety of surface characterization methods. The aim is to explore the relationship between coating composition and structure, how they change in a tribological contact (by tribo-film formation) against NBR counter-body, and tribological performance in terms of friction and wear.

## *Thesis aim*

The aim of this master thesis is to study the tribological performance of carbon alloyed $WS_2$ at rubber contact. The study has been conducted on the effect of microstructure, elevated temperature, crystallinity, and chemical composition on hardness, wear, and friction reduction. A preferable harder, oxidization resistance, durable, and low friction properties of developed coatings are the main goals. The focus to accomplish those goals is to alloy the pure $WS_2$ with carbon and another less studied aspect of the addition of substrate bias during deposition. The main aspect is to deposit and test W-S-C coatings with lower carbon content. Historically, the higher carbon content of around ~50% is commonly used but they are not suitable to provide proper lubrication against rubber contact.

The steps to be executed to accomplish the objective is as follows

1. Sputtered deposition of reference W-S-C coatings with CFUMS equipment with varying C content and application of substrate bias.
2. Proper control of the deposition parameters to achieve the desired C content in the coatings.
3. Characterization of deposited TMD-C film in terms of structure, morphology, mechanical properties, and adhesion.
4. Study of tribological performance of those coatings against NBR rubber contact.
5. Characterization of wear scare and determining of specific wear rate.
6. Study the performance of those coatings at elevated temperatures (200℃).
7. Compare the result with previously studied W-S-C coatings.

## *Thesis organization*

This thesis draft has been divided into 8 chapters. **Chapter 1** introduces the scope of energy savings by reducing frictional loss, the motivation for this study. **Chapter 2** contains the concept of tribology, friction, and wear. **Chapter 3** includes the use of conventional lubricants and the scope of solid lubricants, a brief discussion of coatings as a solid lubricant, TMDs, their inherent issues, and possible remedies, and NBR. **Chapter 4** represents deposition techniques available for this type of coatings, the material used, and characterization techniques used. **Chapter 5** contains details of the experimental procedure. **Chapter 6** contains the discussion and results along with a literature comparison. **Chapter 7** concludes the findings of this work and **Chapter 8** represents the scope of future work.

# Chapter 2

## 2. State of art

### 2.1 Tribology

The science of interacting surfaces in relative motion is called tribology, which originated from the Greek word “tribos”, which means “to rub”. It deals with subjects like friction, wear, and lubrication and is frequently discussed in the context of mechanical engineering. Tribology is vital not just for machine parts and tools, but also for most aspects of our daily lives: walking, using contact lenses, and riding a bicycle, even if we aren't aware of it. Industrial applications, on the other hand, need an understanding of tribological phenomena. Friction and wear reduction may reduce energy and material consumption, extend component lives, minimize operating costs, improve performance, and reduce environmental footprints, among other benefits. For example, the so-called “Jost” study, which created the word tribology, claimed that tribological advances might save the UK more than 500 million GBP per year in 1966 [6]. Similar statistics were later produced for the US (USD 100 billion in 1974) and West Germany ($5 billion DM in 1976) [7]. The figures are, of course, estimates, but optimized tribological techniques might be a mentionable amount, equivalent to a comparable percentage of the gross domestic product of a country.

### 2.2 Friction

Friction is the phenomenon of resistance to relative surface movement. The coefficient of friction is used to measure the severity of the phenomena. It is defined as the ratio of the tangential friction force to the normal force. A schematic of simple friction phenomena has been represented in figure 1.

$$\mu = \frac{F_F}{F_N}$$

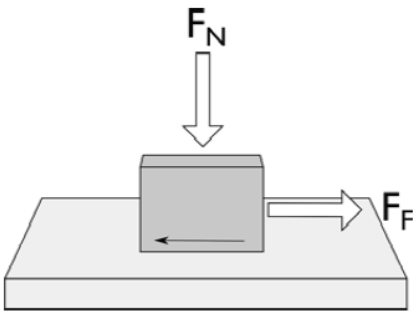

**Figure 1:** Schematic of friction force

There are two types of friction to discuss in general, dynamic or kinetic friction refers to friction between surfaces in motion, whereas static friction refers to resistance to the commencement of sliding. The term "friction" in this study refers to the dynamic friction that occurs when two surfaces slide against one another. The total coefficient of friction can further be divided among adhesive ($\mu_A$) and plowing ($\mu_P$) components.

$$\mu = \mu_A + \mu_P$$

Friction might be caused by a variety of physical processes, including elastic and plastic deformations, fluid mechanics, wave phenomena, and due to specific properties of contacting materials[8]. In classical mechanical engineering, friction has been widely investigated, and there has recently been a strong comeback. Apart from intellectual curiosity, significant engineering demands in a wide range of sectors, from disc drives to automobiles, from space journeys to competitive sports are constantly pushing this sector [9]. One of the most daunting problems here is despite having numerous friction models for both atomic and macroscopic phenomena, it is still difficult to predict the frictional force precisely as it depends on lots of elements of the environment.

## 2.3 Wear

Wear generally refers to the damage to a solid surface, usually involving progressive material loss due to relative motion between the solid surface and contacting substance or substances[10]. The specific wear rate (SWR), which is the worn volume *(V)* divided by the sliding distance *(S)* and the applied load *($F_N$)* for sliding contacts, is frequently used to quantify the wear properties of a system.

$$SWR = \frac{V}{SF_N}$$

Where the specific wear rate has the unit of $m^2N^{-1}$ but is usually given as $mm^3N^{-1}m^{-1}$ or $\mu m^3N^{-1}m^{-1}$. The above equation is a simplified derivation of the Archard model, named after John Frederick Archard, who was one of the first scientists to attempt to explain the wear mechanism. The trivial assumptions are, that local contact occurs when asperities interact, the real contact area is proportional to normal load, and each individual asperity contact is circular[11]. The equation of the Archard model is as follows.

$$Q = \frac{KWL}{H}$$

Where $Q$ is the total volume of wear debris produced. $K$ is a dimensionless constant. $W$ is the total normal load. $L$ is the sliding distance. $H$ is the hardness of the softer contacting surfaces. The wear volume is related to the normal force, the sliding distance, and inversely proportional to the hardness of the softer contact partners, according to the Archard law of adhesive wear. This model doesn't give a clear picture of the adhesion of a material[12] and a literature review of several different wear models can also be found[13].

In general, it may appear that high friction is always associated with high wear and vice versa, but this is not always the case. For example, pure $WS_2$, which is easily sheared and relatively soft, results in low friction but significant wear[14]. The types of wear can be divided into the following categories.

## 2.4 Different types of wear

### 2.4.1 Adhesive wear

Adhesive wear is the undesired displacement and attachment of wear debris and material compounds from one surface to another that occurs during frictional contact between surfaces. There are two forms of adhesive wear that may be recognized. Relative motion, "direct contact," and plastic deformation generate adhesive wear, resulting in wear debris and material transfer from one surface to another. A Cohesive adhesive force might hold two surfaces together even though they are separated by a measurable distance, with or without any actual transfer of material[15].

### 2.4.2 Abrasion wear

When a hard, rough surface slides across a softer surface, abrasive wear develops [14]. It is defined by ASTM International as material loss caused by hard particles or protuberances that are pressed against and travel over a solid surface [16]. The kind of contact and the contact environment is commonly used to classify abrasive wear [17].

### 2.4.3 Surface fatigue wear

Surface fatigue is a kind of general material degradation in which the surface of a material weakens because of cyclic stress. There could be two types of microcracks, superficial and subsurface[15].

### 2.4.4 Fretting wear

Fretting wear is the rubbing of two surfaces in a cyclical pattern. More distinctively, it refers to the reciprocating motion in a very small distance, to be exact, the contacting surface may not even be moved over a comparable measurable distance[18]. It may resemble the occurrence of vibration. Over time, fretting removes material from one or both surfaces in contact. It is particularly common in bearings; however, in most bearings surface hardening combats this issue[19].

### 2.4.5 Erosive wear

Erosive wear is characterized as a very brief sliding action that occurs in a very small-time span. The collision of solid or liquid particles against an object's surface causes erosive wear [20-21]. Through repeated deformations and cutting activities, the attacking particles gradually remove material from the surface [22]. Pipelines commonly suffer from this type of wear [23].

### 2.4.6 Corrosion and oxidation wear

Both lubricated and dry contacts experience corrosion and oxidation wear. Chemical interactions between the worn material and the corroding media are the root cause of this type of wear[20]. Tribo-corrosion is the term for wear generated by a synergistic effect of tribological stresses and corrosion. In a mechanical system, the resulting wear can be the combination of any of those components and will not be distinguished separately in this work.

# Chapter 3

## 3. Lubrication

### 3.1 Lubrication- A walk through

Lubrication is the application of a layer of different materials between moving surfaces in contact to reduce friction and wear. While wear and heat cannot be avoided, they can be reduced to levels that are negligible or tolerable. As friction causes heat and wears, lowering the coefficient of friction between the contacting surfaces can reduce both issues. Lubricant is also used to minimize oxidation and prevent corrosion, as well as to provide insulation in transformers, transmit mechanical power in hydraulic fluid power applications, and seal against dust, dirt, and water[24]. There are three major types of lubricants: Gaseous lubricants e.g. air, helium, Liquid lubricants e.g. oils, water, and Solid lubricants e.g. graphite, grease, Teflon, molybdenum disulfide, etc, a variety of chemicals can also be utilized. The most prevalent are oil and grease. The latter type is made up of oil and a thickening agent to achieve its consistency, with the oil providing lubrication which might be synthetic, vegetable, mineral, or a mixture of them[25]. For liquid lubricant, the process of lubrication can be divided into three categories boundary, mixed and hydrodynamic regime. Although mineral oil-based lubricating oil is the most common one, due to its poor oxidation and thermal stability, they are being replaced by synthetic oil. Their viscosity index and load-carrying capacity are being constantly improved by adding new additives like anti-friction, anti-wear, and viscosity modifiers among others[26]. Till now the most commonly used additives are carbon-based, for example, carbon nanotube, graphite, graphene, and nanodiamond. Although due to having considerable negative impact on the environment they are being replaced by TMD, cupper-based, and boron-based nanoparticles[27]. Vapour phase lubrication is also gaining attention, especially in a smaller system like the microelectromechanical system to minimize the viscous loss, inactive volume, and high temperature seize of liquid lubricants[28-29]. Having some major other issues with a liquid lubricant like higher oxidization rate, unstable viscosity, thermal degradation, toxicity, flammability, and also a frequent need for replacement, it is not recommended for application in the extreme environment and in the delicate system where it could introduce the source of contamination. At the same time, the depleting source of fossil fuel and its negative environmental impact hinders the sustainable future goal[30].

Imparting certain benefits like low cost of production and maintenance, lightweight, consistent efficiency, long-term applicability, and self-lubricating coatings are gaining attention in recent years where all of those benefits can be achieved without altering the base material[31].

## 3.2 Coatings as a lubricant

A coating is a protective layer that is applied to an object's surface, also known as the substrate, and can perform as a solid lubricant. The coating can be applied for ornamental, functional, or both purposes. Although functional coatings can be used to alter the substrate's surface qualities such as adhesion, wettability, reflectivity, anti-reflection, UV protection, self-cleaning, optical properties, sealing, and waterproofing, fire protection, biological barrier, corrosion resistance, our focus in this work will be drawn on the friction and wear reduction. In other circumstances, such as semiconductor device production (when the substrate is a wafer), the coating contributes an entirely new attribute to the completed product, such as magnetic response or electrical conductivity, which is an important aspect of those finished products.

## 3.3 Solid lubricant

A solid lubricant is a powder or thin coating that lowers friction and wear of contacting surfaces in relative motion while also providing damage prevention. Because of the influences of particle form, size, mobility, and crystallographic features of the particles, lubricity provided by solids vary from friction models for liquid lubricants. Solid lubricants are designed to provide a continuous, adhering soft or hard layer on contacting surfaces. Mechanical, electrochemical, and physical systems all can benefit from these films. The mechanism involving its effectiveness is the reduction of the roughness by involving the solid lubricant to adhere to the valleys and leveling the asperity.

Solid lubricants perform a unique role in decreasing wear in situations where liquid lubricants are either impractical or insufficient, such as vacuum, or in space technology. They are necessary for lubrication under severe circumstances. Solid lubricants are frequently used in applications where high specific loads are applied to sliding surfaces in the presence of boundary and mixed frictional regimes, at very low hydrodynamically effective speeds, or when the lubricant must perform over a wide temperature range or in extreme temperatures (e.g., in aviation), in harsh conditions, high-vacuum applications, nuclear reactors, and other applications where contamination by lubricating oils or greases must be avoided, and dry

lubrication in the food industry. Solid lubricants may be made from a variety of materials. Structural lubricants, mechanical lubricants, (reactive) soaps, and chemically active lubricants are the most common types of solid lubricants. The multi-layered lattice structures of structural lubricants (e.g. graphite and metal dichalcogenides) are responsible for their lubricating capabilities. Self-lubricating organic substances (such as thermoplastics and thermosets) and naturally occurring metal oxide films on the outer surface (typically approximately 10 nm thick), chemical surface coatings (produced by a chemical or electrochemical process on the metal surface), and glasses are all examples of mechanical lubricants.

Reactive soaps (stearic, oleic, and palmitic acid salts) in combination with a zinc phosphate coating are common solid metal-forming lubricants. The manufacture of greases is the primary function of soaps (metal salts of fatty acids) in lubrication technology. Soaps can also be generated in situ on a metal surface by a fatty acid attacking the metal chemically. Extreme pressure (EP) and antiwear (AW) additives, as well as other compounds, are chemically active lubricants that interact with the metal surface to form a lubricating or protective layer. The lamellar solids $MoS_2$ and graphite, as well as poly tetrafluoro-ethylene (PTFE) [32] and other fluorine-containing polymers, are examples of common solid lubricants. Magnesium stearate dihydrate (MgSt-D) [33] and hydrogenated castor oil (melting point 86 °C)[34] have also been used as solid lubricants.

Crystal structure, thermal and oxidative stability, volatility, chemical reactivity, melting point, and hardness are all important material qualities for solid lubricants. If thermal degradation of the solid lubricant is to be prevented, heat stability (which is closely related to chemical stability) is essential. Solid lubricants have a temperature range within which they work effectively. Graphite, for example, can endure temperatures of up to 650°C and moderate stresses[35].

Only a few solid lubricants possess the necessary adhesive and cohesive qualities to form an effective lubricating layer with low friction coefficients and a long lifespan. A transporting medium, a bonding agent (such as oils, greases, or water), and/or preparation of the material surface are all required for most solid lubricants. Solid lubricant compositions usually include a solid, a binder, and additives like corrosion inhibitors and solvents[36]. Tribo-layers, also known as tribo-films, occur on surfaces because of structural or chemical changes in the materials in contact. The forces at the contact sites are significant on a microscopical scale,

resulting in high pressures and temperatures, which are likely to cause material changes, forming that tribo-layer. Transfer films are generated when material from one surface is transferred to another, as the name indicates. The function of tribo-films is critical to a system's tribological behaviour and understanding and controlling their function is an important aspect of tribological optimization [37].

## 3. 4 Classifications of solid lubricant

There are mainly four distinctive types of solid lubricant, single component, multicomponent, gradient, and smart coatings. The first one is generally produced by CVD or PVD techniques to reduce the cost and usually contains one of the followings $WS_2$, DLC, $MoSe_2$, TiC, CrC, and CrN-Ag[38]. They utilize the low shear strength of the multi-layered structure to provide low friction. To mitigate the limitation of thermal stability multicomponent coatings could be employed[31] which have a periodic repetition of the distinctive structured component inside the coating. It contains a composite nature within and acts as a diffusion and dislocation barrier and improves mechanical properties[39]. To reduce the drastic change of hardness from coating to the substrate and to facilitate tribo-coating, gradient-layed coatings were developed[40]. For example, TiAlN (hard phase) + $MoS_2$ (soft phase) contains the softer material embedded in harder amorphous material in a depth gradient manner and provides efficient friction reduction on the nanoscale and lower elastic modulus on the microscale. Smart coatings can alter their properties depending upon the environment of applications. Those contain dopped element in the base material, while the base material provides low friction in dry environments and vacuum, the dopped element facilitates low friction in a humid environment[41].

## 3.4 TMD

### 3.4.1 An overview

TMDs are transition metal dichalcogenides which are solid lubricant materials, especially intrinsic solid lubricants, whose crystal structure promotes interfacial sliding/shear to produce low friction and wear in sliding contacts and low torque in rolling contacts [42]. They have the general formula $MeX_2$. The name is applied to compounds in which the metal Me could be Mo, W, Nb, Ta, etc. and the chalcogen X is S or Se or Te. $MoS_2$ is the most well-known compound in the group in tribological applications, while $WS_2$ is also extensively explored.

The multilayer and highly anisotropic structure of these TMDs explains why they have this low friction characteristic. They are made up of metal and chalcogen atom layers, where the layer of metal atoms is sandwiched between two sheets of chalcogen atoms, completing a sandwich layer, as represented in figure 2. A trigonal prism of chalcogen atoms binds each metal atom together [43]. Metal and chalcogen atoms have strong bonds, and a molecular orbital method reveals that all the metal and chalcogen's low-energy orbitals are engaged in bonding inside the sandwich layer [44]. Only van der Waals interactions exist between the sandwiched layers, implying that bonding between sandwiched layers in a particular direction is weak.

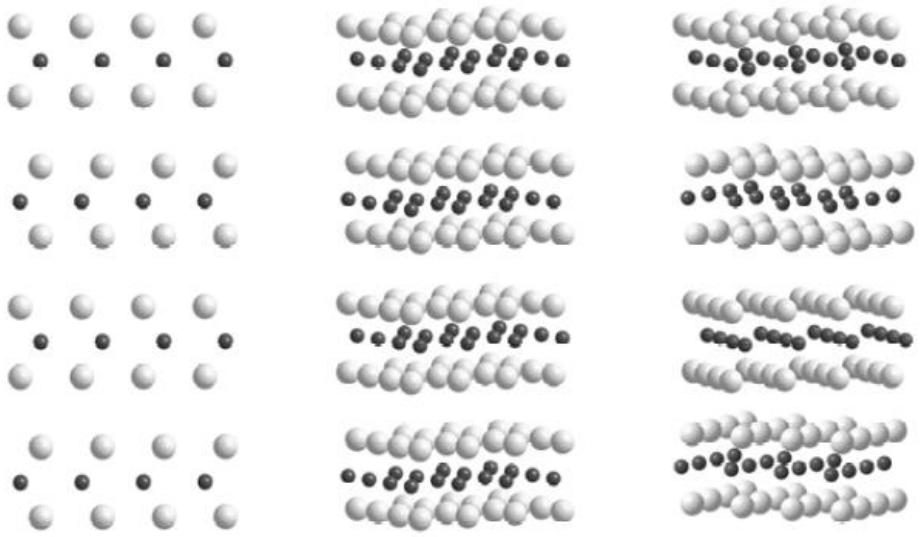

**Figure 2:** Structure of $WS_2$, with 2H-$WS_2$ in 2D and 3D view (left and middle), and turbo-statically stacked $WS_2$ in 3D view (right). W atoms are dark grey and S atoms are light grey. The c axis is vertical in the plane of the paper [37].

Those poor bonding between the sandwich layers results in low shear strength parallel to the planes. $MoS_2$, also known as molybdenite, found naturally as a mineral, has been utilized as such for centuries [45], despite being mistaken for graphite due to macroscopical similarities. As TMDs are known to perform best in vacuum or space settings, most of the work on $MoS_2$, and later $WS_2$, has been concentrated on these applications. This emphasizes a key distinction between graphite and TMD lubrication: graphite requires the presence of intercalating species (such as $H_2O$) to achieve low friction, whereas TMDs are intrinsic lubricants that work best in the absence of such contaminations [46]. TMDs can be oxidized by reactive species such as $O_2$ to the equivalent oxides ($WO_3$, $MoO_3$), which do not have the same low-friction qualities. Furthermore, it has been claimed that the presence of $H_2O$ increases the shear strength of TMDs by strengthening the bindings between the sandwich layers, resulting in increased friction[47-50]. While it is commonly known that $WS_2$-based coatings work better in inert environments

than in ambient air, the impacts of $H_2O$ and $O_2$ are less well understood. Furthermore, the ability of $WS_2$ lubrication to achieve low friction varies not only with the environment but also with the composition and structure of the coating material.

In many circumstances, the mechanical characteristics of pure TMD coatings can be improved, hence mixing TMDs with other materials is a typical solution. TMDs, for example, have been co-deposited with materials with recognized mechanical benefits, such as $TiB_2$ [51], TiN [52-53], CrN [54], or $Sb_2O_3$[55]. The goal is to develop a hard covering with solid TMD lubricant reservoirs. A somewhat different and extensively used approach is to co-deposit TMD with metal, nonmetal elements, and compounds, potentially in minuscule quantities - the phrase "doping" is frequently used. The additional element's purpose is to increase mechanical characteristics by interrupting the TMD's crystallinity. The TMD phase is still in charge of lubricating and low-friction qualities, and the additional element should ideally not interfere in this regard. Metals appear to have been the most common option for the additive element for some reason. Though they aren't perfect, many metals have poor frictional characteristics. Additionally, many metals are vulnerable to the development of oxides, and while certain metal oxides are lubricious, many are abrasive and harmful in sliding contact. The addition of a non-metallic element, such as C or N, is a viable option, and both C and N have been alloyed with TMDs. These element’s oxides are gaseous, which means they may quickly escape the interface without disrupting the $WS_2$ lubrication[37]. There might be two structural forms of TMDs, hexagonal and rhombohedral[56], in this study only hexagonal crystal structures with six-fold symmetry will be discussed.

### 3.4.2 Application of TMDs

In the field of electronics line semiconductors, optics, and sensors TMD has a huge range of applications due to the direct band gap in the structure. They have been recently rediscovered as a replacement for Si and pushed a detailed study in this direction[57]. In mechanical systems on the other hand TMD based additives have long been used as additives for lubricating oil. And TMD coatings as a solid lubricant are being explored for space application[56].

### 3.4.3 Effectiveness of TMD

As it is well known that friction is not a material property but rather a system property, the performance of the TMD crucially depends on its film thickness, crystallinity, stoichiometry, and microstructure. Also, the surrounding environment has a great effect on the performance of TMD. At extreme temperatures, TMD tends to oxidize very quickly[58]. Recently the

deposition of the TMD coatings with sputtering techniques has been reported of having better tribological properties compared to other processes like ion beam deposition[59]. Usually, the sputtered pure TMDs are very soft and appear as standing columns in the micrograph, giving it a lower load-bearing capacity and material transfer to the counter body. During sliding those columns breaks off but gets replenished by the bulk and reorient their basal 002 planes to the sliding direction. The efficiency of this reorientation process depends upon the film thickness, microstructure, and crystallinity of the coatings. Although a very low friction coefficient of pure TMD as 0.002-0.1 has been seen under favorable conditions, the low adhesion causes easy and quick removal of the coating from the substrate. [60-61]. Only a smaller group of TMD compounds have the potential as self-lubricating materials namely $MoS_2$, $WS_2$, $MoTe_2$, etc, all having outer d-orbital filled together with hexagonal lamellar crystallographic structure.

### 3.4.4 Tribo-film of TMD

The formation of a stable tribo-film is necessary for the TMDs to provide low friction, usually, it can be achieved by the reorientation of the 002 basal planes by the application of load to the direction of sliding. At the beginning, usually dominated by running in period, of the running-in period, due to the asperities not being completely deformed a comparatively higher coefficient of friction usually appears before becoming stable later on when the uniform tribo-film is achieved [62]. In the presence of water, that tribo-film gets attacked by hydrogen molecules to the edges of the film where it is unsaturated and forms a strong H-bond and hinders the purpose of the film.

### 3.4.5 Alloying of TMDs

Due to some inherent issues with pure TMDs, alloying them with different elements and compounds has been performed in the past years to impart necessary mechanical strength. To do so, initially, TMDs were alloyed with metal elements like Al, Au, Ni, Cr, and Fe, while particularly Fe was the first element to alloy with $MoS_2$ in the 1970s. Later Ti-doped TMD showed promising results in low temperatures but failed at elevated temperatures. Some issues related to metal element doping is lower deposition rate, comparatively lower thermal stability, abrasive properties of their oxides, and depletion by diffusion. Therefore metal doping did not become viable for upscaling in the industry[56]. Due to those reasons doping with non-metal elements gained popularity, specially alloying with carbon, which is also the aim of this project.

## 3.5 NBR

In this study, the TMD-C coatings will be tested against the NBR, and the performance will be assessed. An oil-resistant synthetic nitrile rubber, commonly known as nitrile-butadiene rubber (NBR), is made from a copolymer of acrylonitrile and butadiene. Its primary uses include gasoline hoses, gaskets, rollers, and other goods that require oil resistance. NBR is made by emulsifying acrylonitrile ($CH_2$=CHCN) and butadiene ($CH_2$=CH-CH=$CH_2$) in water and then polymerizing (linking their single-unit molecules into big, multiple-unit molecules) using free-radical initiators. A physio chemical composition can be seen in figure 3 . The percentage of acrylonitrile in the finished copolymer ranges from 15% to 50%. The rubber gains strength, resistance to swelling by hydrocarbon oils, and decreased permeability to gases as the acrylonitrile concentration rises. However, due to the greater glass transition temperature of polyacrylonitrile, the rubber becomes less flexible at lower temperatures (i.e., the temperature below which the molecules are locked into a rigid, glassy state). Nitrile rubber is typically utilized in places where strong oil resistance is required, such as automobile seals, gaskets, and other objects that come into contact with hot oils. Other apparent uses include rollers for spreading ink in printing and hoses for oil products. NBR is also used in textiles, where it enhances the finish and waterproofing capabilities of woven and nonwoven materials. The hydrogenated form of NBR (abbreviated HNBR) is extremely resistant to thermal and oxidative degradation while remaining flexible at lower temperatures. Nitrile rubber, like styrene-butadiene rubber and other synthetic elastomers (elastic polymers), was developed as a result of research conducted during and between World Wars I and II. In 1934, German scientists Erich Konrad and Eduard Tschunkur of IG Farben invented a set of acrylonitrile-butadiene copolymers known as Buna N. Buna N was developed in the United States as GR-N (Government Rubber-Nitrile) during World War II, and the acrylonitrile-butadiene elastomers that followed became known as nitrile rubber [63].

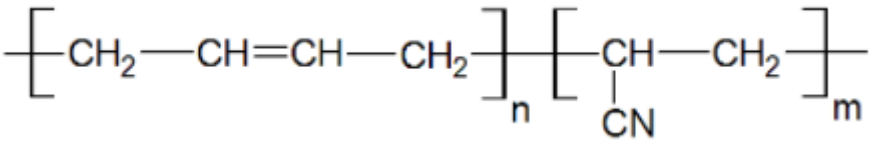


**Figure 3:** Chemical composition of NBR [64].

# Chapter 4

## 4. Coating deposition

### 4.1 Deposition Method

There are several deposition methods available for different thin films and coatings, for functional coatings PVD, CVD, and Electroplating are some of the well-used techniques. Among all of them, PVD has been a proven technique for TMD-C coating deposition, giving promising results.

### 4.2 PVD

PVD (physical vapor deposition) is a vaporization coating process that includes atomic-level material transfer. The following sequence of stages can be used to explain the process. The material to be deposited is transformed into a vapor using physical methods (high-temperature vacuum or gaseous plasma), the vapor is then transferred from its source to a low-pressure location (towards the substrates), and then the vapor condenses on the substrate to produce a thin layer, as represented in figure 4. PVD methods are often used to deposit thin films with thicknesses ranging from a few nanometers to thousands of nanometres. Multilayer coatings, graded composition deposits, extremely thick deposits, and freestanding structures may all be made using it.

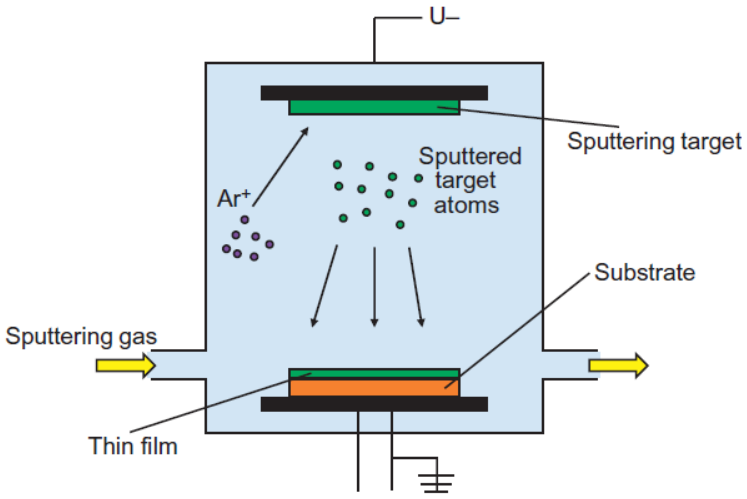


**Figure 4:** Schematic illustration of the physical vapor deposition process.

PVD thin-film technology includes sputtering, electron-beam or hot-boat evaporation, reactive evaporation, and ion plating, among other deposition processes. Processes based on sputtering,

whether by plasma or an ion beam, are similar to PVD methods. PVD is also used to make arc source deposition, which can also be filtered or not[65].

Evaporation and sputtering are the two types of PVD, respectively. In the sputtering process, the plasma molecule is bombarded on the target surface and makes the target molecule escape from the surface. While in evaporation the target molecule escapes through the thermal energy provided to the target.

## 4.3 Sputtering

Sputtering is one of the most substantial PVD processes, in which bombarding, energetic, and atomic-sized particles cause the physical vaporization of atoms from a surface. Sputter deposition allows for more control over the composition of multielement films and a wider range of materials can be deposited [65]. Being initially described by Wright in 1877, sputter deposition of films was only made possible by the low vacuum required for its functionality. Although Edison developed a general sputter deposition technology for depositing silver onto wax picture cylinders in 1904, magnetron sputtering did not become widely employed in the industry until 1974. The use of sputter deposition has accelerated the development of repeatable, stable, and long-lasting vaporization sources for manufacturing. Planar magnetron sputtering has become the most extensively utilized sputtering arrangement due to the employment of a magnetic field that limits the mobility of the secondary electrons close to the target surface. It was developed from the construction of the microwave klystron tube during WWII, as well as Kesaev and Pashkova's (1959) research on confining arcs and Chapin's (1974) research on building the planar magnetron sputtering source [66-67].

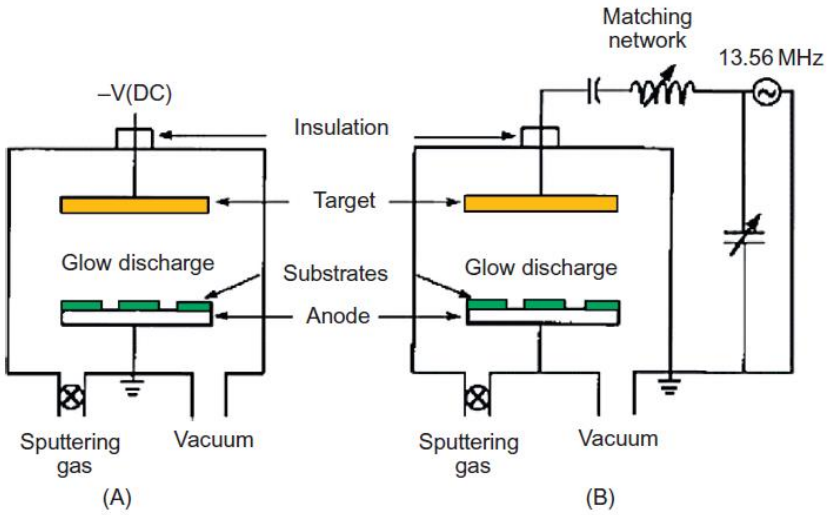


**Figure 5:** Schematic diagram of the principles of (A) direct current (DC) and (B) radio-frequency sputtering systems [68]

In this deposition process, a good vacuum is first achieved (<$1.5*10^{-8}$ bar) then a sputtering gas (usually argon) is introduced into the chamber resulting in pressure reaches to approximately $4*10^{-6}$ bar. The argon gas gets ionized and creates a distinctive colorful plasma. This plasma-based sputtering is currently the most prevalent type of sputtering, in which positive ions (usual argon) are driven to the target, which is at a negative potential with regard to the plasma. At increasing pressures, the ions are subjected to physical and charge-exchange collisions, resulting in a spectrum of ion and neutral energies attacking the target surface. The ions reach the target surface with energy determined by the potential difference between the surface and the place in the electric field where the ions are generated at low pressures. The power supply to the target can be usually two types, direct current or in the form of radio frequency as shown in figure 5.

Sputter deposition can be used to deposit elemental material films as well as alloy films while maintaining the target material's composition. This is possible because the material is removed layer by layer from the target, which is one of the process's key advantages. This enables the atom-by-atom deposition of more complicated alloys such as Al, Si, and Cu for semiconductor metallization[69] and metal Cr, Al, and Y alloys for aircraft turbine blade coatings [65], and in our case the deposition of TMD-C.

## 4.4 Magnetron sputtering

Magnetron sputtering coating is a physical vapor deposition (PVD) coating technology that is primarily used for depositing metals, alloys, compounds, and other materials with a thickness of up to 5 micrometers onto a variety of substrates [70]. It has several significant benefits over other vacuum coating processes, which has led to a wide range of commercial applications ranging from microelectronic production to simple ornamental coatings. High deposition rates, ease of sputtering any metal, alloy, or compound, high-purity films, extremely high adhesion of films, excellent coverage of steps and small features, ability to coat heat-sensitive substrates, ease of automation, excellent uniformity on large-area substrates, such as architectural glass, are just a few of the benefits of it.

When power is delivered to a magnetron, a negative voltage of generally 300V or more is applied to the target as a working principle. This negative voltage pulls positive ions to the target surface, generating a lot of kinetic energy at the same time. When a positive ion collides with atoms at the surface of a solid, energy transfer happens. Primary recoil atoms can be generated if the energy delivered to a lattice site is larger than the binding energy. These atoms

can then collide with other atoms and disperse their energy via collision cascades. If the energy transferred in a direction normal to the surface is greater than three times the surface binding energy, sputtering occurs (approximately equal to the heat of sublimation). One of the probable outcomes of ion bombardment of a surface is the sputtering of a target atom. Aside from sputtering, the emission of secondary electrons from the target surface is another significant phenomenon. The glow discharge (plasma) can be sustained by these secondary electrons. The target materials for the sputtering process are nearly limitless, ranging from pure metals that can be sputtered with DC power to semiconductors and isolators that require either RF power or pulsed DC. Deposition can be done with single or multielement targets in either nonreactive (inert gas only) or reactive (inert and reactive gas) discharges[71]. Different essential working parts can be seen in figure 6.

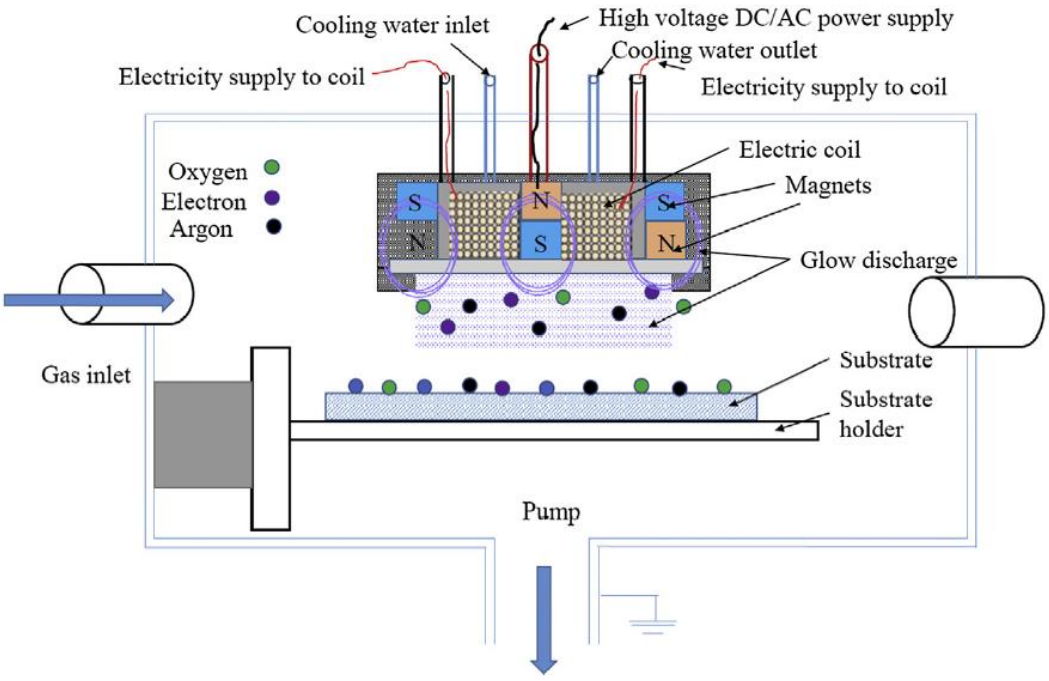


**Figure 6:** Schematic diagram of the mechanism of magnetron sputter coating machine[70].

For the deposition of TMD films, magnetron sputtering is a tried-and-true method. Many TMD researchers in numerous disciplines used magnetron sputtering to prepare their samples. Both examples are from tribological and semiconduction points of view. For example, Wang J et al. used this process to deposit $WTe_2$ for an ultrafast thulium-doped fiber laser[72]. However, for tribological applications, this above process is frequently confined to the production of small-scale specimens but large-scale uses of this technique for structural applications have also increased in recent years. For example, research for TMD film deposition with bigger and comparatively more complex components has been done in recent years by Vuchkov T et al.

[73]. Magnetron sputtering provides several benefits over other processes, making it favorable for the deposition of TMD films. TMD films are typically used in applications that need high purity, rapid deposition, and vast area coverage, all of which are possible using magnetron sputtering. Consequently, this approach will be used to deposit film in this work.

## 4.5 Balanced and unbalanced magnetrons

The magnetron sputtering techniques can be divided into two types depending upon the type of magnetron used, balanced, and unbalanced. For the balanced type, the magnetic flux via the pole faces of the outer poles and through the pole face of the inner pole, as shown in Figure. 7A. The magnetic trap confines the plasma immediately in front of the cathode target if the condition is met. As a result, ions have little impact on the substrate. This is useful when depositing on heat-sensitive surfaces, for example. Window and Savvides created an unbalanced magnetron to boost the ion flux to the substrate [74]. It is based on the strengthening or weakening of magnetic flux through one of the poles, resulting in a magnetic circuit unbalance. Two types of unbalancing are defined by Window and Savvides [74]. As seen in Figure. 7B, all field lines originate from the central magnet, with some not going into the annular magnet. The unbalanced field lines in this situation are directed toward the chamber walls, resulting in low plasma density near the substrate.

As seen in Figure. 7C, all field lines originate from the annular magnet, with some not crossing through to the central magnet. These uneven field lines reach all the way down to the substrate. Some secondary electrons can go away from the target and toward the substrate along these magnetic field lines. As a result, the plasma is not tightly restricted to the cathode target zone and might flow out toward the substrate and the ion current density in the region of the substrate increases dramatically[74], allowing a substrate bias to control the energy of the ions attacking the substrate during film formation.

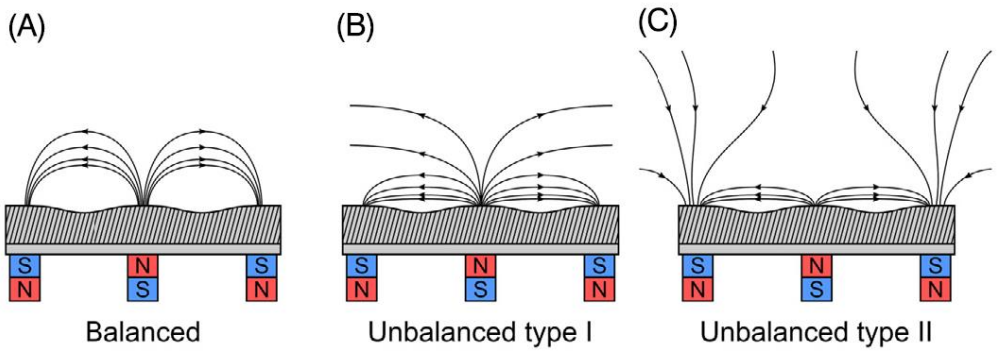


**Figure 7:** A schematic of the magnetic design commonly used in magnetron sputtering discharges. The three cases, (A) all the field lines originate from the central magnet and pass into the annular magnet (Balanced), (B) all the field lines originate from the central magnet, with some not passing into the annular magnet (Unbalanced type I), and (C) all the field lines originate from the annular magnet, with some not passing into the cylindrical central magnet (Unbalanced type II)[75].

# Chapter 5

## 5. Experimental procedures

### 5.1 Deposition technique used

The adaptive tribological response of the co-sputtered TMD-C nanocomposite coatings was analyzed by Voevodin [76], indicating three prominent phases in the nanocomposite structure responsible for the low friction properties, crystalline $WS_2$, amorphous C, and WC. The author concluded that in ambient air (higher humidity) the low COF was mainly maintained by amorphous C while in dry $N_2$ and vacuum this performance was carried out by $WS_2$. Further study by Polcar [77-79] contradicted the previous study proving that TMD phases were also governing the friction in the ambient air. Those authors studied various systems of TMD-C (W–S–C, Mo–Se–C, W–Se–C, Mo–S–C) deposited by Radio Frequency Magnetron Sputtering which is suitable for small-scale laboratory deposition and has several disadvantages for industry scale deposition like depositing on the 3D complex substrate, additional instrumentation, lower deposition rate accumulating increased cost, and deposition variation caused by different power supply and control unit resulting in varying current density and voltage applied to the target. The method used in this project is semi-industrial size close field unbalanced magnetron sputtering (DC mode) also overcomes the requirement of a single

composite target associated with RF which is not feasible on an industrial scale[80]. Semi-industrial-sized deposition equipment, Teer UDP 650/4 (Teer Coatings Ltd., Droitwich, UK), has been used in this project. Its 4 planner target holders were equipped with one $WS_2$, one Cr, and two carbon (C) targets (380 × 175 × 8 mm), all with 99.9% purity. The two C targets are justified as C has a lower sputtering yield than the other two materials[81]. The target to substrate distance was kept at 25 cm as it has been seen to produce coatings with better tribological properties at higher temperatures in the literature[82].

## 5.2 Substrate preparation

AISI H11 steel rectangular-cuboid with a hardness of Rockwell-c ~ 53, was used as a primary substrate. The surface intended for coating deposition was polished with gradually finer grid-sized SiC paper followed by 6 mm and 1 mm diamond suspension to achieve a surface roughness <20 nm. Si wafer was also prepared for depositing coatings for Grazing Incidence X-ray Diffraction (GIXRD), Scanning Electron Microscope (SEM), and Nanoindentation analysis. Both types of substrates were ultrasonically cleaned for 10 mins and dried with hot air before placing them in the deposition chamber.

As a usual process of PVD, all the targets and the substrates were sputtered-cleaned. The total time for this was 40 and 20 minutes for each substrate and target respectively with different power supply systems. The substrates were supplied with a pulse bias voltage (Advanced Energy Pinnacle plus, Fort Collins, CO, USA, 600 V, 250 kHz reverse time of 1.6 μs) and a DC power supply of 1000W (Advanced Energy Pinnacle, Fort Collins, CO, USA) was connected to the targets.

## 5.3 Details of power settings of the equipment

The process of sputter cleaning was followed by the actual deposition of the coatings. The total time of deposition for each substrate was 120 minutes of which the first 10 minutes were the deposition of the Cr interlayer with power of 2000W. The next 10 minutes were utilized for the deposition of a gradient layer of Cr which was done by gradually decreasing the power supplied to the Cr to zero while increasing it for the C and $WS_2$ or only the $WS_2$ target to their designated values presented in table 1. In total four distinct coatings were prepared by varying the power supply to the target and substrate (WS0V, WS50V, WSC1005, WSC1010). The power settings for those coatings can be seen in table 1. For the entire deposition time, a base pressure of 0.4 Pa was maintained with a constant supply of Argon (Ar) gas.

| Sample | C1 Power(W) | C2 Power(W) | WS2 Power(W) | Cr Power(W) | Substrate Bias(V) |
|---|---|---|---|---|---|
| WS0V | 0 | 0 | 800 | 0 | 0 |
| WS50V | 0 | 0 | 800 | 0 | -50 |
| WSC1005 | 250 | 250 | 1000 | 0 | 0 |
| WSC1010 | 500 | 500 | 1000 | 0 | 0 |

**Table 1:** Parameters for deposition timespan from 20-120 minutes

## 5.4 Type of testing employed

Several different characterization techniques were employed to investigate different aspects of the deposited coatings. To reveal the chemical composition of the coatings a wavelength dispersive spectroscopy (WDS) was used (Oxford Instruments, High Wycomb, UK). The thickness, surface, and cross-sectional morphology were investigated by a field emission scanning electron microscope (FESEM). A grazing incident X-Ray diffraction (GIXRD) was performed on the coatings deposited on the Si substrate to understand the crystal structure. Co-Kα radiation ($\lambda = 0.17902$ nm) was used at a 2-degree incident angle to measure the intensity in the scanning range of 2 thetas of 5-90 degrees and the scan step size was 0.025° with 2-second exposition per step. One of the most important aspects of a coating-substrate system, the adhesion, was investigated by a scratch test apparatus (Rtec instruments). A conical diamond tip with a radius of 0.2 mm was used and applied in progressive force mode, ranging from 2-70 N in values with a 10N/mm loading rate. It is to note that this test method doesn't give a measurement of the fundamental adhesion force between the coating and substrate but rather gives an engineering measurement of practical adhesion strength affected by the complex interactions of the test parameters and is only primarily applicable to the brittle damage mode between the coating and substrate[83]. To define the failure mode an optical microscope ((Alicona Infinite Focus, Raaba, Austria) has been used followed by the scratch operation. The mechanical properties like hardness and reduced elastic modulus of the deposited coatings were investigated by a nanoindentation test (Nanotest, Micro Materials Ltd.,Wrexham, UK). The apparatus was equipped with a Berkovich diamond pyramid indenter with a load of 3 mN. This load parameter was selected for making the indentation depth smaller

than 10% coating thickness as recommended[84]. The coefficient of friction of the coatings were determined by Rtech Instrument in reciprocating operation mode against NBR balls with 10mm diameter. All the tests were repeated at least 2 times to check for reproducibility. The data were collected for room temperature (RT) 25℃ and 200℃ (HT). The wear profile has been analyzed through 3D scanning using white light interferometry followed by Gwyddion [85] processing software and wear volume was calculated by the Origin software package [86]. The image of the wear track obtained from that optical microscopy was imported to Gwydion processing software, the surface was labeled, the polynomial background was removed, and cross-sectional profile data was obtained and exported to the origin software package to remove the noise and evaluate the cross-sectional profile area. The wear volume was calculated by multiplying the profile area by the length of the wear track. At least 2 tests were performed for each sample with each condition to check for reproducibility (RT- Room Temperature- 25℃, HT-High Temperature- 200℃). According to ASTM G133-05, 3 profile was evaluated for each wear track and profile areas were averaged. $W_v = W_a*L$, here $W_v$ is the average wear volume (calculated from the origin in $mm^3$), $W_a$ is the wear profile area, L is the length of the wear track (6mm in this case), and the specific wear rate (SWR) has been calculated by the following equation, $SWR = W_v/F*S$, Where F is the normal force exerted by the pin in N. S is the total length traveled by the pin for the whole duration of the COF test. Given that for every sample and condition, the frequency of the reciprocal motion was 5 Hz and the test has been run for 200s, L as 6 mm, and S has been calculated as 12m.

# Chapter 6

## 6. Results and discussion

This project is dedicated to having a better understanding of the mechanical properties and tribological performance of carbon alloyed transition metal dichalcogenide coatings against NBR rubber, tailored to the percentage of C content and its microstructure. In particular, the W-S-C system's performance against rubber contact has been the focus. To accomplish this goal, 4 different coating samples have been prepared with varying alloying content and tested with respective characterization techniques to understand different properties. Their

tribological performance has been compared with bare steel (H11) and an investigation has been done on the effect of temperature (RT and HT) on the performance

## 6.1 Chemical compositions

WDS equipment has been employed to reveal the chemical composition of the coatings. The experiment confirms the main agenda of varying carbon content in the coatings, WS0V, WS50V, WSC1005, and WSC1010, with ~6.6%, ~6.6%, ~18.5%, and ~27.6% respectively in normalized atomic percentages. Although in table 1 it has been mentioned that no power to the C target has been applied to form the first two coatings there have been mentions of residual C content in the literature by the cross-contamination in the sputtering chamber and similar percentages have also been reported[81]. Table 2 contains weight percentage of elements of the AISI H11 steel. The use of substrate bias does not affect the C content on the deposition as evident between the first two coatings as represented in table 3.

| C | Mn | Si | Cr | Ni | Mo | V | Cu | P | S | Fe |
|---|---|---|---|---|---|---|---|---|---|---|
| 0.35-0.45 | 0.20-0.60 | 0.80-1.25 | 4.75-5.50 | 0.3 | 1.10-1.60 | 0.30-0.60 | 0.25 | 0.03 | 0.03 | Balance |

**Table 2:** Chemical composition (weight percentage) of H11 steel[87]

| Sample | ~C% | ~S/W | ~O% | S% | W% |
|---|---|---|---|---|---|
| WS0V | 6.6± 0.5 | 1.6 | 2.7± 0.2 | 56.1± 0.2 | 34.2± 0.2 |
| WS50V | 6.6± 0.1 | 1.5 | 8.6± 0.1 | 51.1± 0.4 | 33.3± 0.5 |
| WSC1005 | 18.5± 0.4 | 1.3 | 5.1± 0.4 | 42.5± 0.1 | 33.2± 0.1 |
| WSC1010 | 27.6± 0.3 | 1.4 | 3.9± 0.1 | 39.1± 0.1 | 28.9± 0.1 |

**Table 3:** S/W ratio and the Oxygen and Carbon percentage (atomic) of the samples

The Chalcogen/Transition-metal ratio (S/W in this case) plays a vital role in the performance of the TMD-C coatings. All 4 coatings produced are sub-sociometric with respect to S percentage according to table 3. Meaning that in the bulk coating W-S system, the S/W ratio is

not directly 2 as in compound $WS_2$. This is a common occurrence in the CFUMS with some exceptions with reactive sputtering with $H_2S$ gas. It has been concluded that due to the mass difference between W and S, the lighter one, S, gets scattered on a larger scale than the other, hindering it to reach the substrate, resulting in a lower (<2) S/W ratio [88]. It is evident from the above figure, comparing the first 2 coatings, WS0V, and WS50V, that substrate bias influences the S/W ratio by promptly decreasing it. The substrate bias is most likely to be resulted in an aggregated Ar+ ion in the vicinity of the substrate surface causing the preferential re-sputtering of the lighter S atoms[81]. The addition of the C content for the following one, WSC1005, has further reduced the S/W ratio drastically. The application of power to the 3 magnetron generates denser plasma near the substrates due to the interaction among them. As we have an unbalanced magnetron in close field configuration, although in C-alloyed coatings no substrate bias was used, it is very likely that the Ar ions from the dense plasma bombard the substrates causing preferential sputtering or even bombardment-induced thermal evaporation of the S atoms. The last sample WSC1010, with further increased C content, showed the opposite trend, having an increase in S/W ratio, more likely to happen that the ratio between the incoming bombarding ions and the incoming film-forming species is lower as compared to the WSC1005. This effect could be seen as the C atoms protecting the S atoms from being preferentially sputtered

The O content in the coatings is not negligible as mentioned in the previous literature on higher C content Mo-Se-C system[81] although the overall decreasing trend of the percentages with increased C content is the same as seen before. The effect of substrate bias is drastic on the O percentage, between the first two coatings, WS0V, and WS50V, only the use of negative 50V of substrate bias on the following one increases the O content by almost 4 times might also be tailored to the difference in morphology. The residual $O_2$ in the deposition chamber or contamination in the targets are the most probable cause for the presence of O in all of the coating samples [89]. As the higher C content increases the compactness and reduction of the porosity in the coatings the surface makes it less accessible by the O, hence reducing the percentage.

## 6.2 Structural characterization

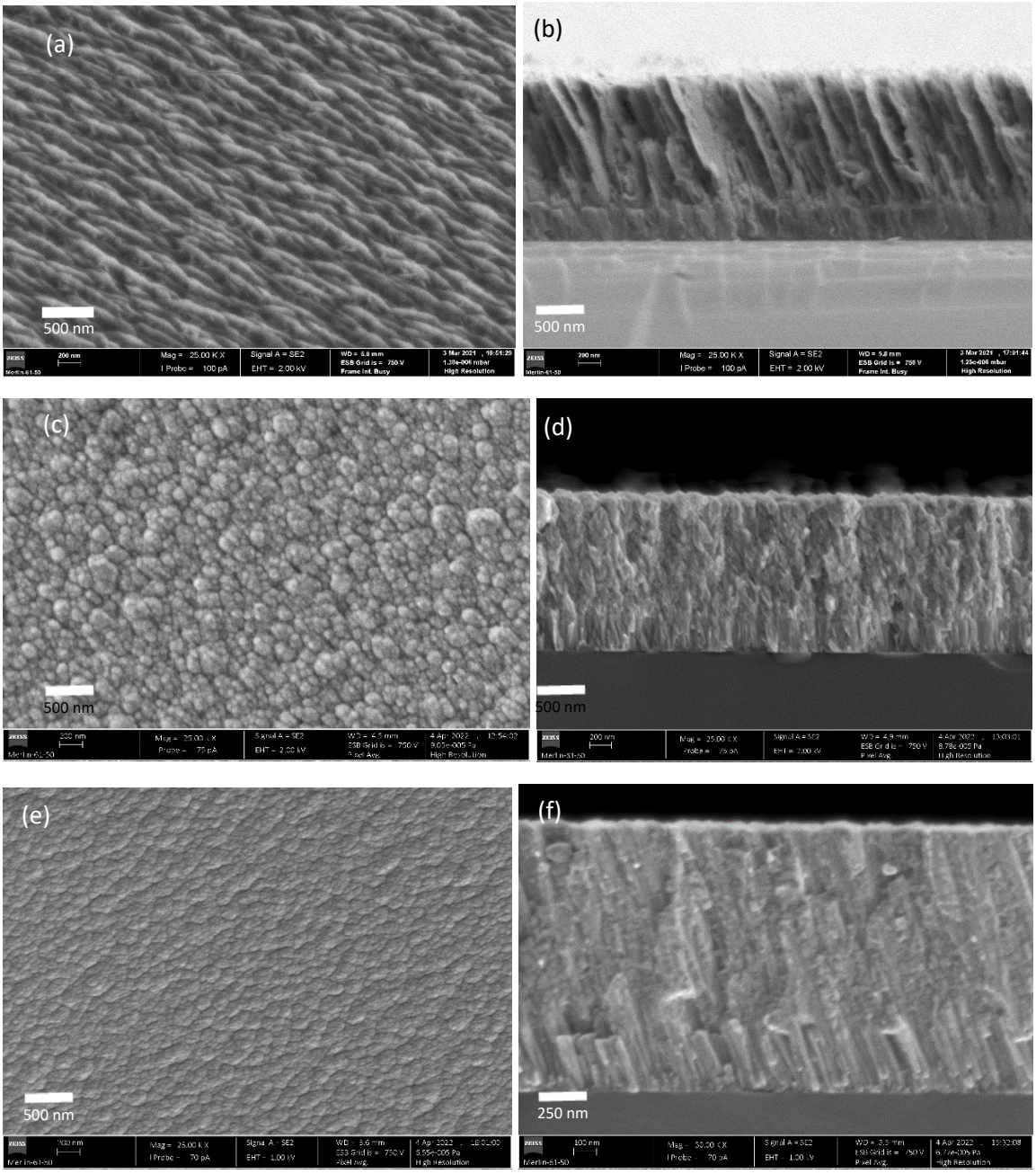

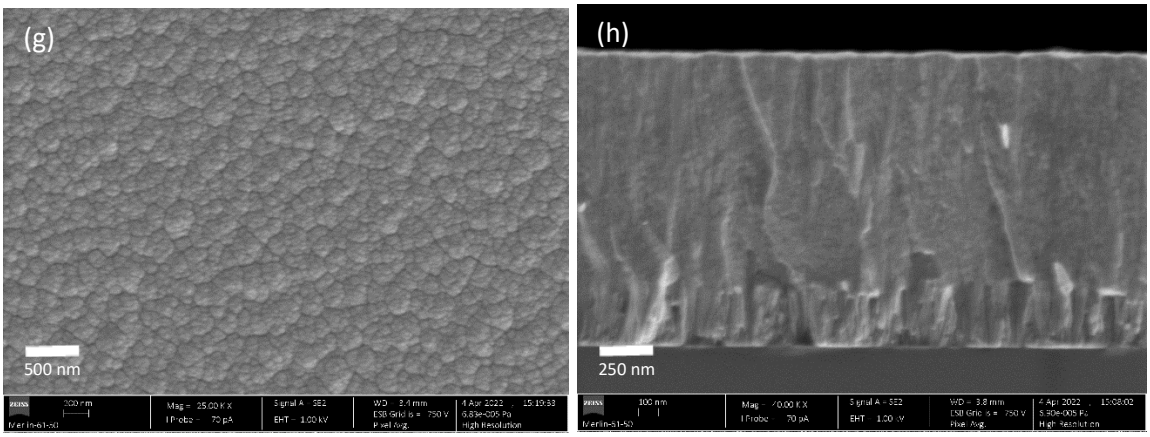


**Figure 8:** SEM image of the as-deposited coatings. (a), (c), (e), (g) are the top views and (b), (d), (f), (h) are the cross-section view of the WS0V, WS50V, WSC1005, WSC1010 respectively.

In the figure 8(a), unalloyed WS0V shows a sponge-like surface morphology which is very common in almost all pure TMD systems [90]. In figure 8(b) the cross-section morphology, there is an evident presence of columnar structure as a elongated surface feature. Indicating a very porous structure like previous studies[82, 91]. Again, in the structural morphology, substrate bias has a great effect. As is seen by comparing WS0V and WS50V, the application of 50V bias changed both surface and cross-sectional morphology from sponge-like to cauliflower and to reduced columnar structure respectively. An increase in surface mobility is probably the cause behind this, the diffusion of sputtered atoms is more likely to happen in a substrate-biased condition by the increase in temperature associated with it. The addition of C content in WSC1005 with ~18.5% C, shows a denser and more featureless structure, indicating fewer voids in the column and more cauliflower-like surface morphology. In the last sample, WSC1010 with ~27.6% C, top surface appearance is almost the same as WSC1005, with more denser, almost solid featureless cross-section. An important to be noted here, the Mo-Se-C system with 33% C in the previous study[81] showed a less featureless (i.e. less dense cross-section) despite having a higher percentage of C.

| Sample | Coating Thickness (μm) | Interlayer Thickness (μm) |
|---|---|---|
| $WS_2$ | 1.17 | 0.33 |
| $WS_2$50V | 1.15 | 0.33 |
| WSC1005 | 0.91 | 0.29 |
| WSC1010 | 1.21 | 0.32 |

**Table 4:** Thickness of as-deposited coatings

From table 4, all the coatings show similar thickness, while WSC1005 has the lowest one probably due to the lowest S/W ratio.

## 6.3 Crystalline characteristics

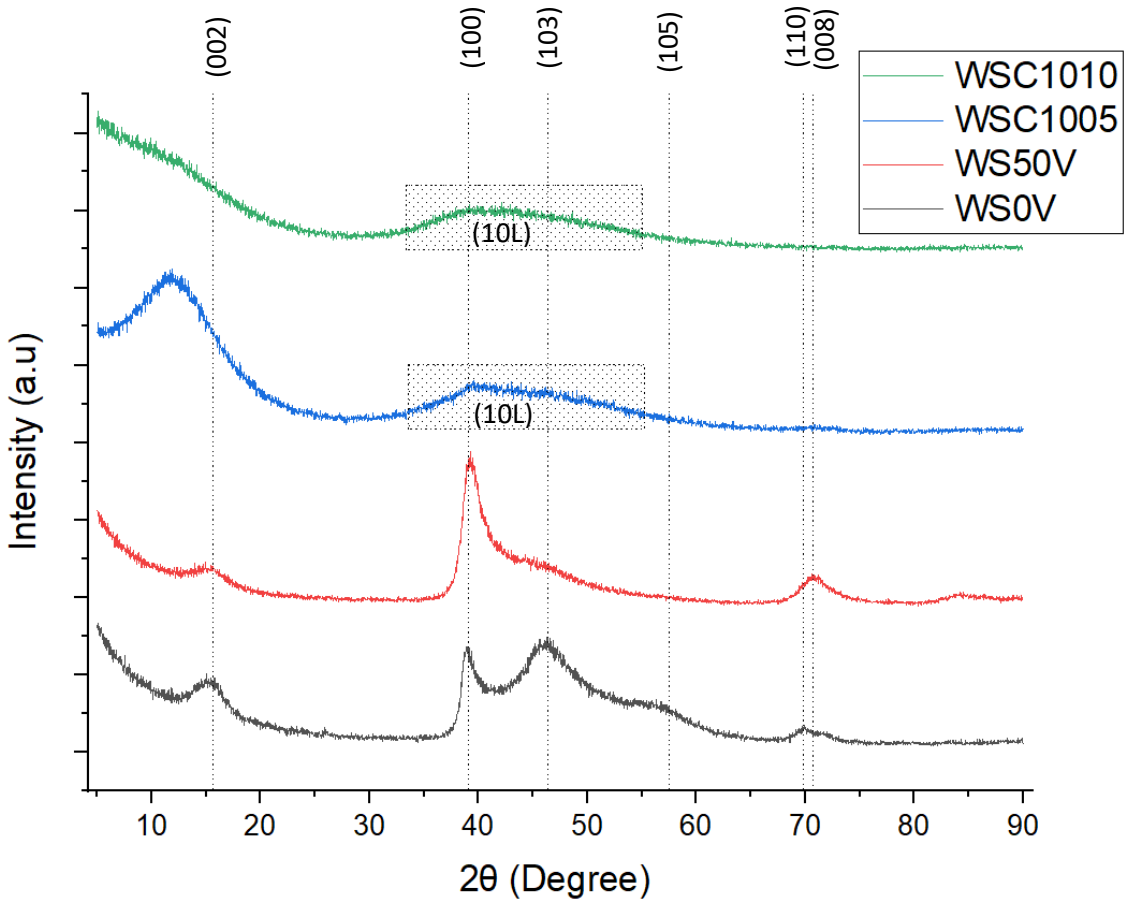


**Figure 9:** GIXRD diffractogram of the samples

In the grazing incident mode, only a few hundred nanometres of the coatings have been analyzed and Si and Cr peaks are not visible for that reason in figure 9. Several comparatively stronger picks have been seen for crystalline $WS_2$, the crystal planes orientations are as follows basal (002) at 2θ ~16°, (100) at 2θ ~38°, (103) at 2θ ~46°, (105) at 2θ ~58°, (110) at 2θ ~69°,

and (008) at 2θ ~71° (ICSD reference no: 01-084-1398). Due to the smaller penetration depth, the Cr peaks are not so evident in the diffractogram. Peaks at a higher angle (2θ ~69° and ~71°) have been flattened out for the C alloyed coatings, resulting in distortion in the crystal structure. As the sharp picks translate into a more crystalline structure, here WS0V represents the most crystalline structured coatings among all. The loss of crystallinity is evident in the C alloyed coatings has the broader peaks generally mean more amorphous structure[92]. A turbostratic stacking of planes has been seen in the WSC1005 and WSC1010 along 2θ span of ~33°-55° of the (10L) plans (with L values of 1,2, 3,…..) which is common for sputtered TMD systems [93][94], meaning the usual hexagonal stacking might be suffered from rotation or translation due to the weak interaction between the TMD layers. (002) plan which is nearly parallel to the substrate is known for being tailored to the easier shearing properties of TMD[81] and has a sharp peak for the WS0V. The addition of the substrate bias has a negative effect on crystallinity of WS50V by making this peak broader. Further addition of the C in WSC1005 and WSC1010 increases this effect meaning the WS0V coating should have the best tribological performance among all followed by WS50V and other C alloyed coatings. WS50V has a strong pick at (100) plane which is nearly perpendicular to the sliding direction and needs to reorient itself in the contact region to provide better tribological performance.

## 6.4 Mechanical characterization

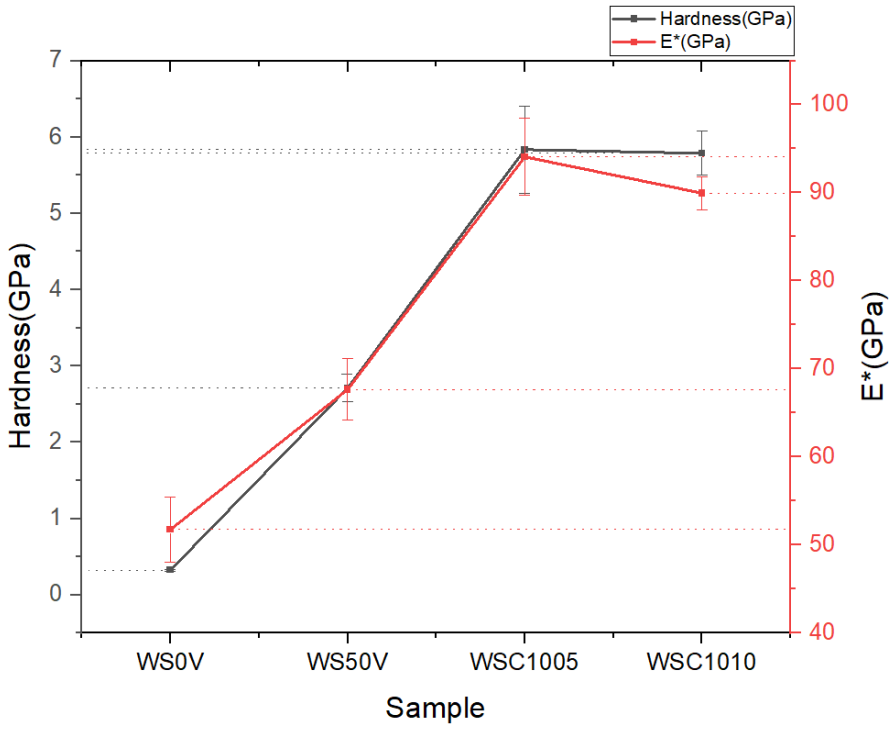


**Figure 10:** Hardness and Reduced elastic modulus (E*) of the coatings

Nanoindentation has been performed to identify two distinct mechanical properties, hardness, and reduced elastic modulus precisely and presented in figure 10. A huge jump in terms of hardness has been seen by the introduction of substrate bias. As in typical W-S coatings deposited by a similar method in the previous study reported a hardness of 0.32 GPa[95] and has been confirmed in our study, a value of almost 8.5 times has been accounted for just by 50V of substrate bias in the second sample, in agreement with the evidence of increased compactness and reduced S/W ratio mentioned before. The increase in reduced elastic modulus is also significant here. Due to the introduction of substrate bias E* increased from ~52 to ~67 GPa. From WS50V to WSC1005 the hardness and E* increased a lot, again in agreement with the aforementioned effect of compactness and S/W ratio. Apart from that, the decrease in the S/W ratio means a larger amount of W present in the coatings and more possibility of formation W-C phase which is harder than $WS_2$, further enhancing the hardness[96]. The upward trend of the hardness and E* is contradicted by the last sample WSC1010, which can be explained by its increased S/W ratio compared to WSC1005. A higher S/W ratio favors the formation of the crystalline $WS_2$ phase with inherently low hardness[89], resulting in reducing the overall hardness and E* of the last sample slightly. The hardness value has been seen to further increase with increasing C content of the W-S-C system of 49% and 64% respectively in the previous studies[3]

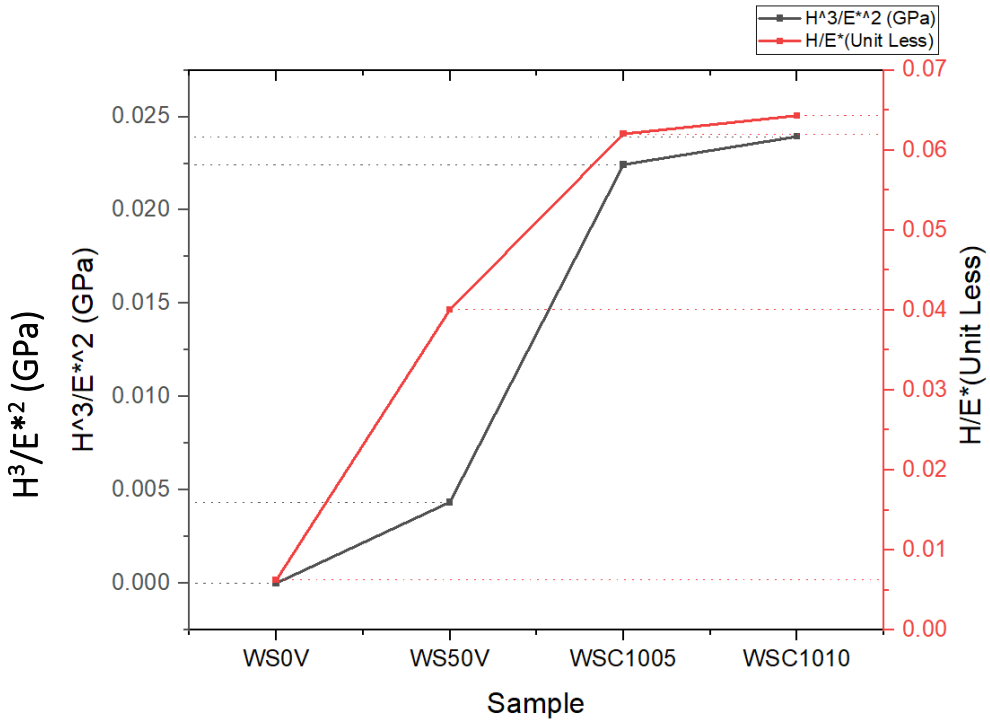

**Figure 11:** Failure properties of the coatings

Here in figure 11 two mechanical properties of material regarding failure could be seen in figure 11, $H^3/E^{*2}$ (H and E* representing hardness and reduced elastic modulus respectively) representing the resistance to plastic deformation[97], meaning higher values are desirable, often translated into lower wear rate. On the other hand, H/E represents the elastic strain of failure[98], also a higher value is desirable for less failure. In the above graph, an upward trend is evident with the addition of substrate bias and by further increasing the C content in the coating

## 6.5 Adhesion Test

A mechanical test of adhesion has been performed on the coatings and represented in figure 12.

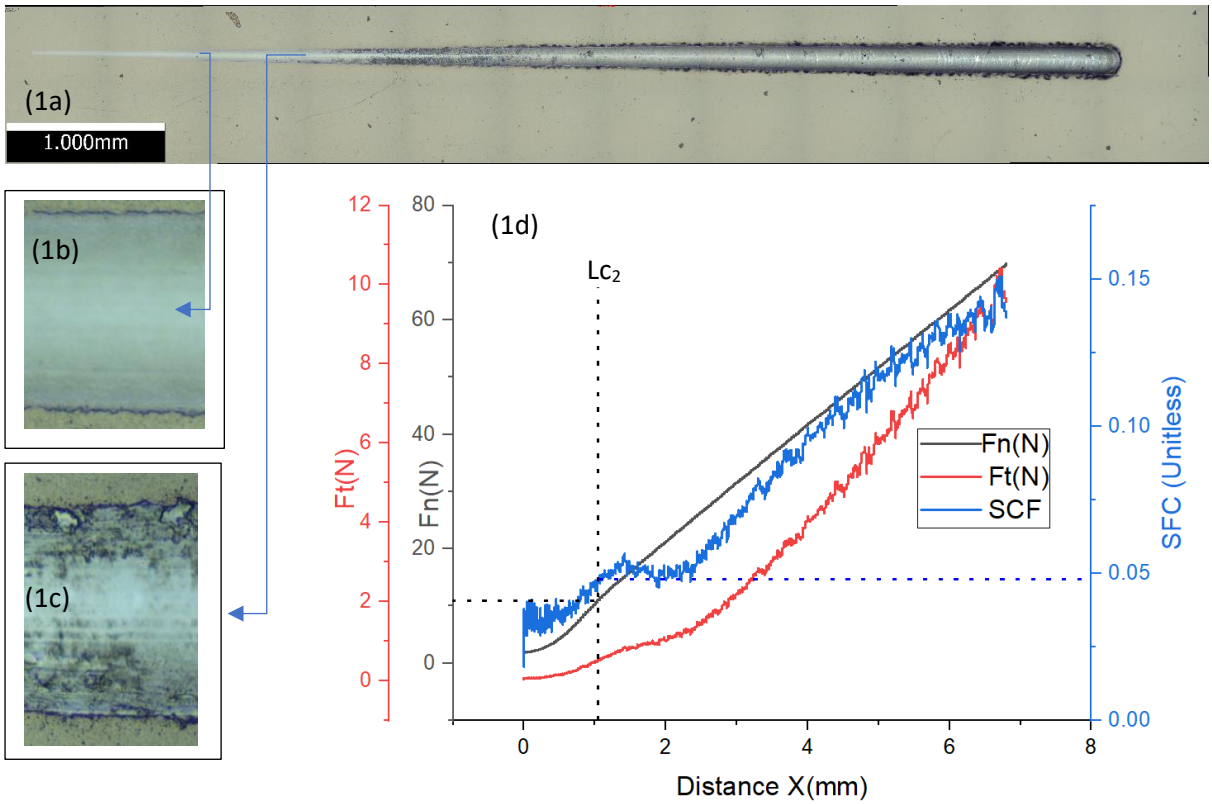

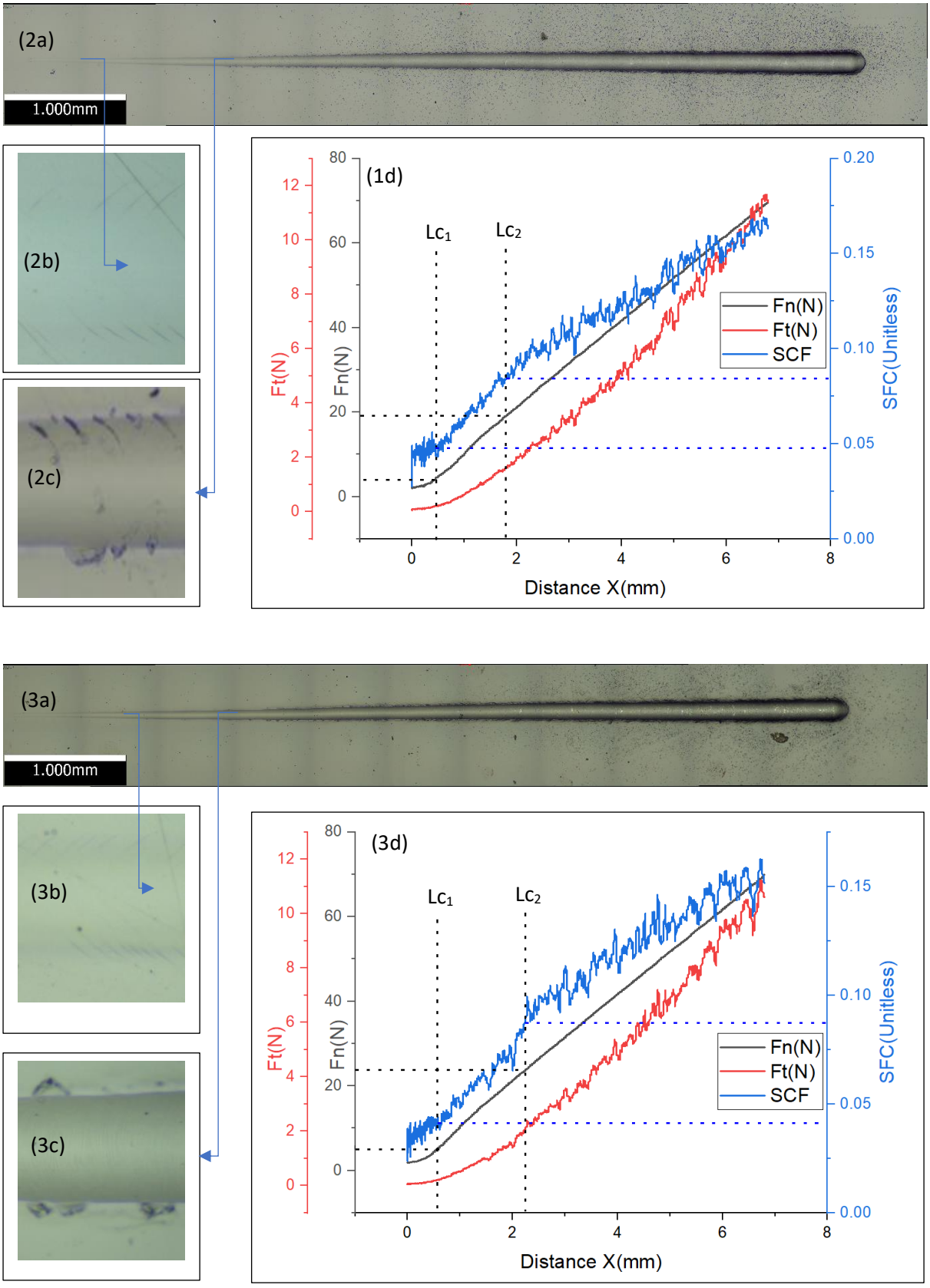


**Figure 12:** (1a), (2a), and (3a), are the image of the scratch whole track for $WS_2$50V, WSC1005, and WSC1010. (2b), (3b) are the micrograph of the wear tack at critical load ($Lc_1$) for WSC1005, and WSC1010. (1b), (2c), and (3c) are the zoomed image of the wear tack at critical load ($Lc_2$), (1d), (2d), (3d) representing the distance vs normal load ($F_n$), tangential

load ($F_t$), and Scratch coefficient of friction (SFC) of the $WS_2$50V, WSC1005, and WSC1010 respectively.

| Coatings | $Lc_1$(N) | $Lc_2$(N) |
|---|---|---|
| WS50V | | ~11 |
| WSC1005 | ~4 | ~19 |
| WSC1010 | ~5 | ~24 |

**Table 5:** Critical loads for the coating scratch test

A quantitative coating adhesion scratch test has been performed according to ASTM C1624-05 standard, a commonly used method for this type of coating with brittle damage nature and presented in table 5. The critical crack load (Lc) was used to differentiate between the adhesive and cohesive failure modes of the coatings. $Lc_1$ has been designated for the cohesive failure (chevron crack) which occurs inside the coating region and $Lc_2$ for buckling and spallation which occurs due to adhesive failure between coating and substrate at the interface.

The test has not been performed on WS0V coatings as it is inherently very soft. For WS50V, there is no cohesive failure has been seen. $Lc_2$ starts at a relatively lower length of 1.2 mm with a load of 11 N, observed from the optical microscopy image of scratch length, figure 12(1b). which can be further supported by graph figure 12(1d), with a sharp change of trend in the SCF. Later on only the severity of the $Lc_2$ failure increased when spallation started to appear not only on the edge of the scratch track but also inside at around 1.9 mm length, as indicated by figure 12(1c).

In WSC1005 both $Lc_1$ and $Lc_2$ have been seen. First, $Lc_1$ appeared at around 0.43mm with a normal load of 4 N as a form of forwarding tensile chevron tensile crack, indicated by figure 12(2b). At a length, of around 1.81 mm the recovery spallation occurred with $Lc_2$ of 19 N. Both $Lc_1$ and $Lc_2$ load positions can be supported by the figure 12(2d) graph with a sharp change in the trend of the Scratch coefficient of friction (SCF) curve.

For WSC1010 both $Lc_1$ and $Lc_2$ only appeared for higher normal loads compared to WSC1005, which appeared at around 0.53 and 2.2 mm respectively indicated by the images figure 12(3b)

and figure 12(3c) respectively. Again, both length positions are supported by the SCF curve in figure 13(3d).

A general trend of increasing critical load for both cohesive and adhesive can be observed with increasing C content in the coatings, indicating a better cohesive and adhesive strength. WS50V, a comparatively softer (lower harness) coating, showed only failure in the interface of the coatings and substrate, probably it is not brittle enough for cracking inside the coating region. For relatively harder coatings, i.e. WSC1005 and WSC1010, both failures occurred but at relatively much higher critical load. So, it is safe to say with increasing C content the failure mode shifts from adhesive to cohesive.

## 6.6 Tribological characterization

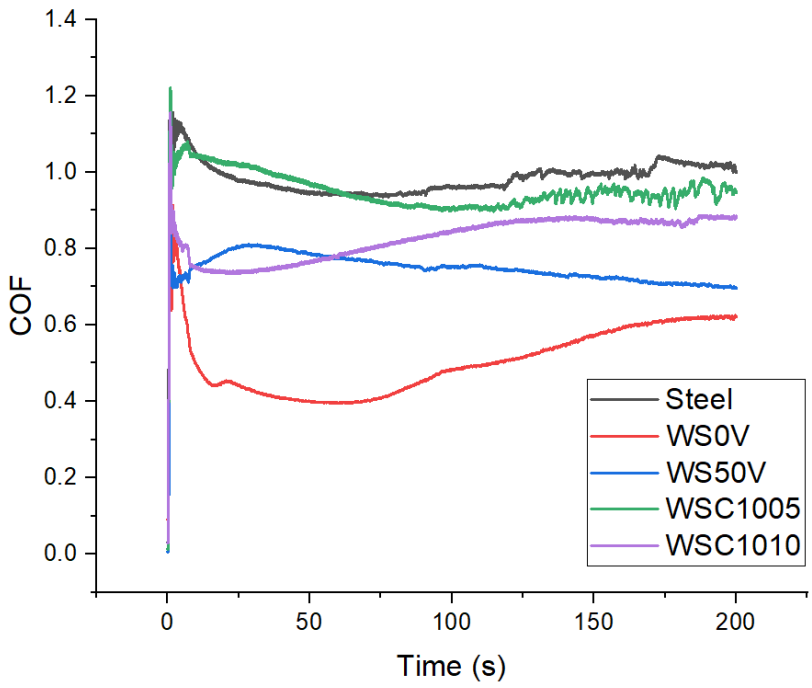


**Figure 13:** Coefficient of friction Vs time for RT(~25℃)

At RT the lowest coefficient of friction is given by pure WS0V (~0.61) followed by WS50V (~0.7), WSC1010(~0.88), WSC1005(~0.95), and H11 steel(~1.01), as presented in figure 13. As we know the pure WS0V contains the highest value of S/W ratio, and therefore is expected to have the lowest COF. It has been investigated that the highest depth of the wear track (~1.1 μm) of the WS0V could reach the coating thickness (1.16 μm) at some points, indicating the

initial drop and then gradually rising of the COF for WS0V as a result attributed by loss of coating itself from the substrate at some areas. WS50V has a higher COF compared to WS0V probably because there should be some wear for stabilizing the tribo-film, the WS50V is probably hard enough not to allow any significant wear thus the lubricious W-S tribo-film couldn't be established. On the other hand, coatings with higher C content showed a quite similar, higher COF, probably due to similar morphology and crystallinity. Although giving WSC1010 a slightly lower value than WSC1005, which can be explained by having a higher S/W ratio for WSC1010. All of the coatings performed better than bare H11 steel.

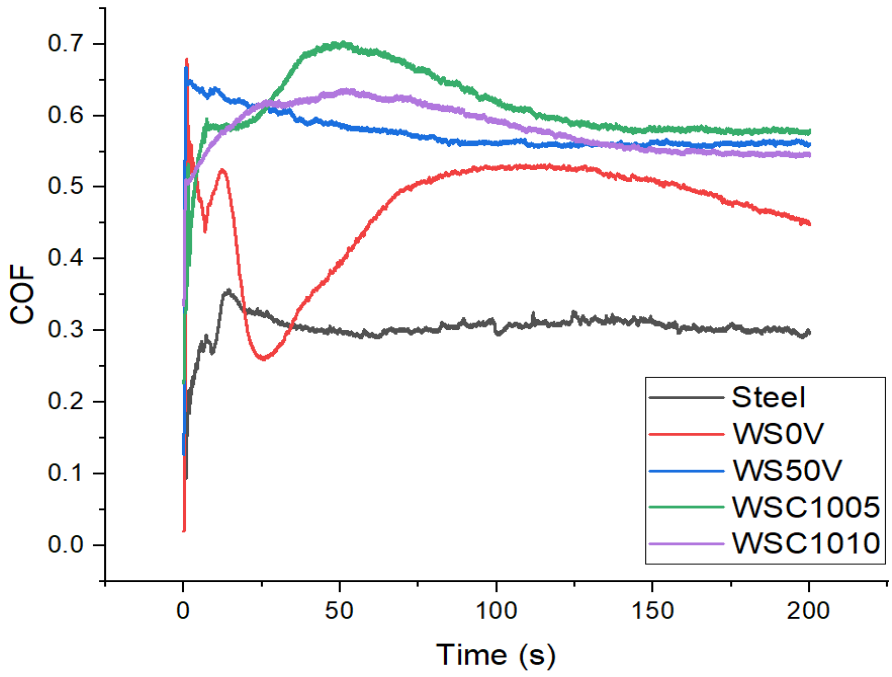


**Figure 14:** Coefficient of friction Vs time for HT(~200℃)

At HT all the coatings have improved their tribological performance by reducing COF. WS0V gave the lowest COF among coatings (~0.45), as presented in figure 15. Even a reducing trend has been seen at the end of the test, indicating it could further reduce if the test would continued for a longer cycle. Followed by WSC1010(~0.54), $WS_2$50V(~0.56), and WSC1005(~0.58), giving quite similar values. For all coatings, the COF values were reduced at the HT. A possible explanation could be the reduction of relative humidity in the proximity of the testing rig which facilitates the reduction of the shear strength of the TMD phases [62] and the additional thermal energy could facilitate the reorientation of the $WS_2$ tribo-layer to the direction of sliding

promoting friction reduction [99]. H11 has the lowest COF, probably due to the formation of a thin rubber layer that is soft and lubricious at high temperatures[100]. The better performance for the H11 steel is very likely due to the better adherence of the rubber material to its surface. This can be due to the different morphology between the polished steel sample and the coating. In the case of the coating the voids between the cauliflower feature can entrap the rubber-based material, i.e. it will be out of contact. As for the WS0V coating, due to its lubricity, a lower COF was initially observed but there was an increase. In this case, due to the wear of the coating, the formation of rubber-based tribo-films is not possible.

## 6.7 Wear rate analysis

| Sample | ~SWR ($mm^3$/Nm) at RT | ~SWR ($mm^3$/Nm) at HT |
|---|---|---|
| WS0V | $7.5*10^{-5}$ | $10.3*10^{-5}$ |

**Table 6:** Specific wear rate of WS0V

Interestingly only quantifiable wear has been seen on WS0V coatings both on RT and HT and presented in table 6. The SWR was calculated and presented in the above table, which is comparable with the previous literature[3, 95]. Tribology of TMD against rubber is a very special case of a scenario where it has been seen that for more compact (WS50V) and higher C-contained coatings (WSC1005, WSC1010) the rubber is more likely to wear out rather than coatings itself. It is evident from the table that at a higher temperature of 200℃ the specific wear rate is significantly higher than the room temperature. Probably due to the acceleration of the formation of the softer $WS_2$ in the interface by the diffusion of the species from the bulk coatings. This increase in the wear could have resulted from the accelerated oxidation of $WS_2$, being the main reason. Furthermore, at HT the temperature at the contact point is more likely to be higher than the applied 200℃ facilitating the oxidization of the $WS_2$ phase and promoting the wear rate.

## 6.8 Analysis of the wear scar

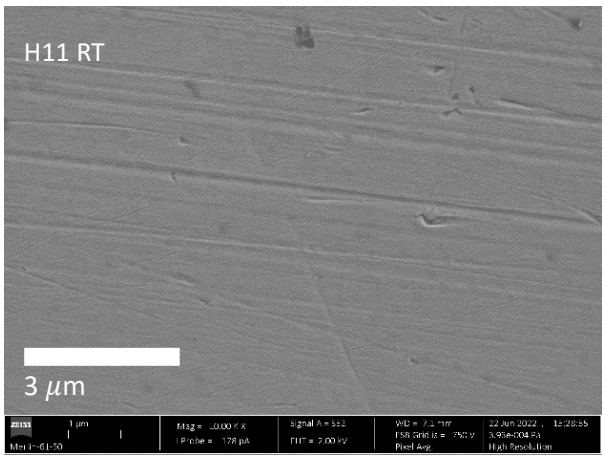


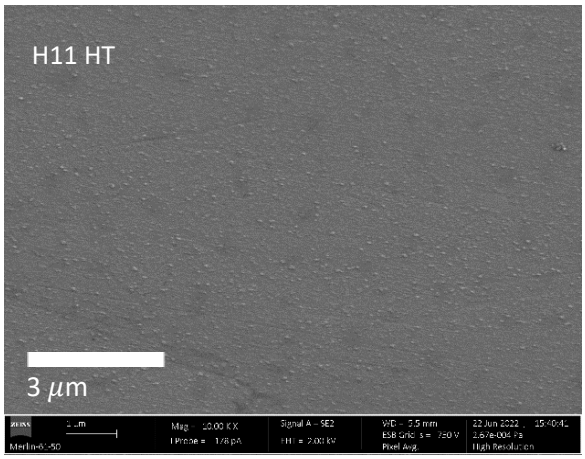


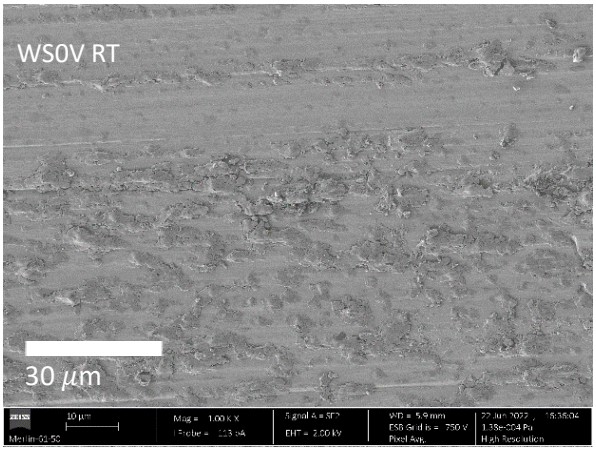


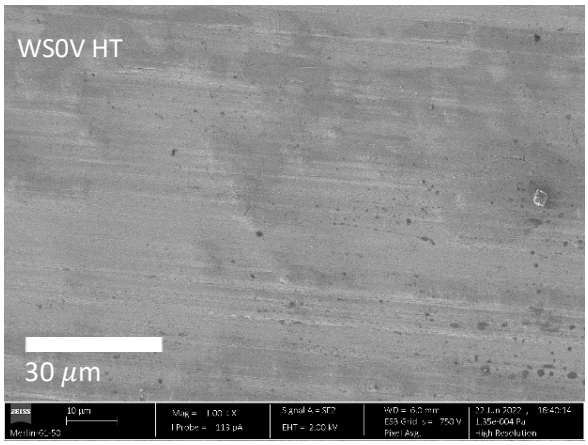


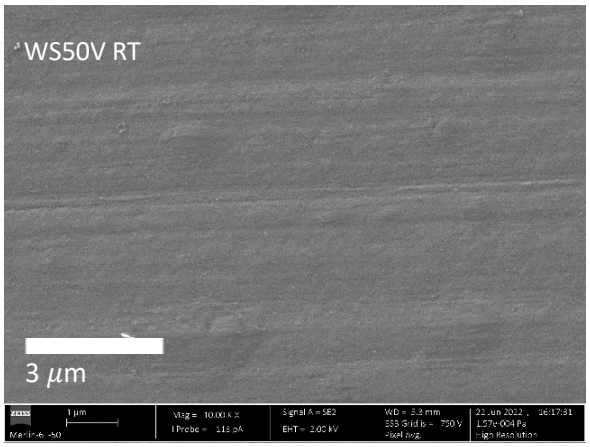


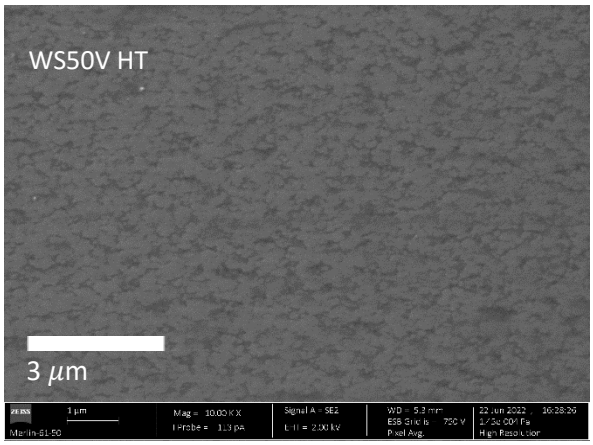

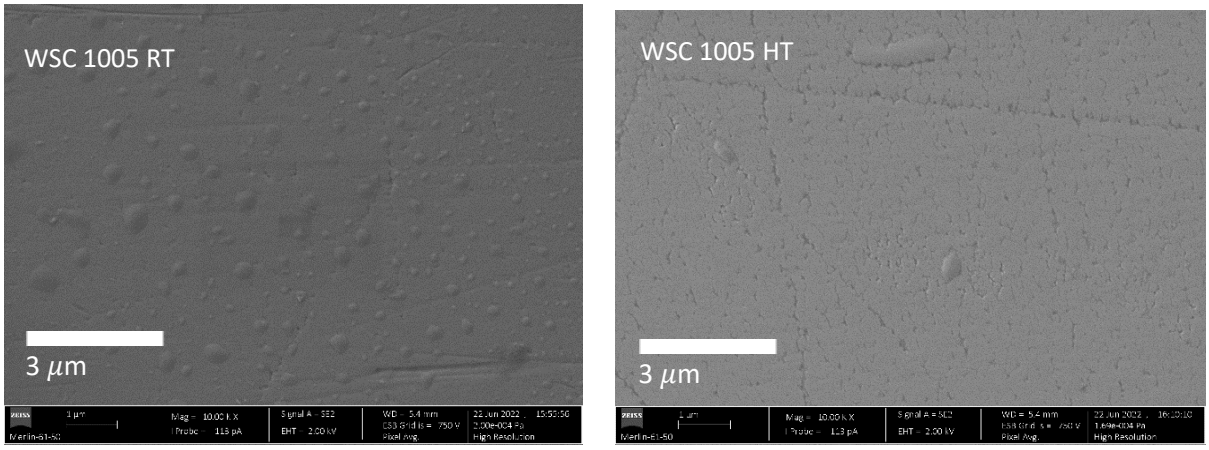


**Figure 15:** SEM image of the wear track

To reveal the morphology of the wear scar the SEM of the wear track has been performed for both room and high-temperature test conditions and presented in figure 15. For a given sample both RT and HT images are of the same magnification for the benefit of comparison. At RT the H11 steel wear scar appeared very smooth and some track line is visible. On the other hand at HT some black dots as a pattern is visible together with some blister-like convexity which is probably formed by the material transfer from the rubber counter body. According to the Bowden and Tabor model the friction coefficient depends on the normal load, real contact area, and the shear strength of the tribo-film[101], on the other hand, the area of each contact is proportional to the force to hardness ratio. As it is very likely that the shear strength of the thin rubber layer is very low thus providing lower friction. Figure 15 doesn't contain WSC1010 as there is no significant difference with WSC1005.

For the WS0V there is much more wear debris in the scar but not in an arranged manner for the RT due to the low adhesion probably the material from the coatings transferred and attached to the rubber counter body. WS50V had a lower S/W ratio than WS0V, hence lower $WS_2$ formation chance in the contact point, and needed to reorient the TMD phases to the sliding direction. But probably due to the lower hardness and reduced elastic modulus of NBR resulting in lower contact stress was not enough for fully formation of the TMD phase at the contact point. At HT comparatively lower COF had been achieved. The main difference here between RT and HT is the darker appearance in the latter one, suggesting much more rubber material transfer for the coating. The local temperature at contact points in HT is more likely to be more than 200℃ and it has been seen in the literature [102] that at high-temperature NBR

goes under heat accumulation which reduces the tensile and tear strength. For C alloyed coatings at HT, the surface appeared much smoother than the RT. The cauliflower-like appearance in the as-deposited coatings is much flattened out on the letter one.

# Chapter 7

## 7. Conclusion

In this work, the mechano-tribological performance of the C-alloyed TMD coatings has been investigated. In a semi-industrial deposition unit, four different coatings have been prepared and tested against NBR rubber, leading to the following conclusions.

- Substrate bias plays an important role in altering the properties of non-alloyed coatings, even in very small amounts.
- A Higher S/W ratio is beneficial for lower COF but affects the mechanical properties of the coatings
- Resistance to plastic deformation and strain of failure both increase with introducing additional C in the coatings.
- Failure shifts from adhesive type to cohesive type by increasing C in the system.
- By introducing a small amount of substrate bias (-50V in this case) and further addition of C in the TMD system the compactness increases (evident by the SEM image).
- Crystallinity decreases by additional C in the system as expected.
- The C-alloyed coatings (~18.5% and ~27.6%) in this study didn't show much difference in terms of mechanical and tribological performance.
- In C-alloyed coatings, more rubber material is transferred to the coatings than other way around.
- For the non-alloyed coatings, it is easier to replenish the removed $WS_2$ from the contact by the counter body.
- For all the coating the initial higher COF could result from the presence of O on the outer surface.
- Among all four coatings, WSC1010 has more balanced mechanical and tribological properties.
- The performance of bare H11 steel against NBR at elevated temperatures needs further investigation.

# Chapter 8

## 8. Future work

The following future work could be recommended

- Use of different substrate biases to understand its effect more properly.
- The introduction of substrate bias and C together in the system.
- Testing the performance at dry nitrogen.
- EDS mapping of NBR counter ball to assess the material transfer properly.
- Alloying WS with higher C content and assessing its performance.
- The friction of H11 steel with different roughness could be tested against NBR at 200℃ to fully understand the hypothesis of thin layer NBR presence on the H11 surface.

# Reference


[1] A. S. Pouzada, E. C. Ferreira, and A. J. Pontes, “Friction properties of moulding thermoplastics,” *Polymer Testing*, vol. 25, no. 8, pp. 1017–1023, Dec. 2006, doi: 10.1016/j.polymertesting.2006.06.009.

[2] K. Holmberg and A. Erdemir, “Global impact of friction on energy consumption, economy and environment,” *FME Transactions*, vol. 43, no. 3, pp. 181–185, 2015, doi: 10.5937/FMET1503181H.

[3] Geet Raju, “Tribological study of TMD coatings for rubber applications Submitted in Partial Fulfilment of the Requirements for the Degree of Master in Materials Engineering Geet Raju,” University of Coimbra, Coimbra, 2015. Accessed: Jan. 24, 2022. [Online]. Available: https://estudogeral.uc.pt/bitstream/10316/39086/1/Tribological%20study%20of%20TMD%20coatings%20for%20rubber%20applications.pdf

[4] D. E. (David E. Packham, *Mould sticking, fouling and cleaning*, vol. 13. Rapra Technology Ltd, 2002. Accessed: Jan. 24, 2022. [Online]. Available: https://chemtec.org/collections/processing-methods-polymers/products/978-1-85957-357-0

[5] J. Caessa, T. Vuchkov, T. bin Yaqub, and A. Cavaleiro, “On the microstructural, mechanical and tribological properties of Mo-Se-C coatings and their potential for friction reduction against rubber,” *Materials*, vol. 14, no. 6, Mar. 2021, doi: 10.3390/ma14061336.

[6] H. P. Jost, “Lubrication (tribology) education and research,” London, 1966.

[7] H. P. S. J. Jost, “Tribology’s big bonus 1,” *Industrial Lubrication and Tribology*, vol. 33, pp. 216–226, 1981.

[8] F. Philip. Bowden and David. Tabor, *The friction and lubrication of solids*. Clarendon Press, 2001. Accessed: Jan. 24, 2022. [Online]. Available: https://global.oup.com/academic/product/the-friction-and-lubrication-of-solids-9780198507772

[9] H. Olsson, K. J. Åström, C. Canudas De Wit, M. Gäfvert, and P. Lischinsky, “Friction Models and Friction Compensation,” *European Journal of Control*, vol. 4, no. 3, pp. 176–195, Jan. 1998, doi: 10.1016/S0947-3580(98)70113-X.

[10] “ASTM-G40 | Standard Terminology Relating to Wear and Erosion | Document Center, Inc.” https://www.document-center.com/standards/show/ASTM-G40/history/2001%20EDITION (accessed Jul. 06, 2022).

[11] J. F. Archard, “Contact and Rubbing of Flat Surfaces,” *Journal of Applied Physics*, vol. 24, no. 8, p. 981, Jun. 2004, doi: 10.1063/1.1721448.

[12] V. Popov, “GENERALIZED ARCHARD LAW OF WEAR BASED ON RABINOWICZ CRITERION OF WEAR PARTICLE FORMATION,” *Facta Universitatis, Series: Mechanical Engineering*, vol. 17, no. 1, pp. 39–45, Mar. 2019, doi: 10.22190/FUME190112007P.

[13] M. HC, “Wear modelling: Evaluation and characterisation of wear models,” Michigan, 1994.

[14] E. Rabinowicz, *Friction and Wear of Materials (2nd Edition)*. 1995. Accessed: Jan. 24, 2022. [Online]. Available: https://www.wiley.com/en-ie/Friction+and+Wear+of+Materials%2C+2nd+Edition-p-9780471830849

[15] "WEAR," *https://en.wikipedia.org/wiki/Wear#Wear_types_and_mechanisms*. 2022.

[16] "Standard Terminology Relating to Wear and Erosion," in *Annual Book of Standards*, vol. 03.02, ASTM, 1987, pp. 243–250.

[17] "Friction, LASM ubrication, and Wear Technology ," in *ASM Handbook*, vol. 18, ASM International, 1917. Accessed: Jan. 25, 2022. [Online]. Available: https://www.asminternational.org/search/-/journal_content/56/10192/27533578/PUBLICATION

[18] R. B. (Robert B. Waterhouse, *Fretting corrosion,* [1st ed.]. Oxford ;New York: Pergamon Press, 1972.

[19] C. Lu-Minh, P. Njiwa, K. Leclerc, Y.-M. Chen, J. Delgado, and P.-F. Cardey, "Effectiveness of greases to prevent fretting wear of thrust ball bearings according to ASTM D4170 standard," *Results in Engineering*, vol. 14, p. 100468, Jun. 2022, doi: 10.1016/J.RINENG.2022.100468.

[20] G. Stachowiak and A. Batchelor, "Engineering Tribology," *Engineering Tribology*, 2006, doi: 10.1016/B978-0-7506-7836-0.X5000-7.

[21] J. R. (Joseph R. ) Davis, "Surface engineering for corrosion and wear resistance," ASM International, 2001, pp. 61–67.

[22] M. K. Padhy and R. P. Saini, "A review on silt erosion in hydro turbines," *Renewable and Sustainable Energy Reviews*, vol. 12, no. 7, pp. 1974–1987, 2008, Accessed: Jan. 25, 2022. [Online]. Available: https://ideas.repec.org/a/eee/rensus/v12y2008i7p1974-1987.html

[23] C. A. R. Duarte, F. J. de Souza, and V. F. dos Santos, "Mitigating elbow erosion with a vortex chamber," *Powder Technology*, vol. 288, pp. 6–25, Jan. 2016, doi: 10.1016/J.POWTEC.2015.10.032.

[24] N. S. and A. M., "Lubrication and Lubricants," in *Tribology - Fundamentals and Advancements*, InTech, 2013. doi: 10.5772/56043.

[25] W. Cash, "What Is Lubrication?" https://www.machinerylubrication.com/Read/28766/what-is-lubrication (accessed Jan. 25, 2022).

[26] M. de B. Bouchet, J. M. Martin, C. Matta, and L. Joly-Pottuz, "The Future of Boundary Lubrication by Carbon Coatings and Environmentally Friendly Additives," *Advanced Tribology*, pp. 598–599, 2009, doi: 10.1007/978-3-642-03653-8_193.

[27] M. Kalin, J. Kogovšek, and M. Remškar, "Nanoparticles as novel lubricating additives in a green, physically based lubrication technology for DLC coatings," *Wear*, vol. 303, no. 1–2, pp. 480–485, Jun. 2013, doi: 10.1016/J.WEAR.2013.03.009.

[28] N. H. Forster, "Rolling Contact Testing of Vapor Phase Lubricants—Part III: Surface Analysis©," *http://dx.doi.org/10.1080/10402009908982183*, vol. 42, no. 1, pp. 1–9, Jan. 2008, doi: 10.1080/10402009908982183.

[29] D. Berman and J. Krim, “Surface science, MEMS and NEMS: Progress and opportunities for surface science research performed on, or by, microdevices,” *Progress in Surface Science*, vol. 88, no. 2, pp. 171–211, May 2013, doi: 10.1016/J.PROGSURF.2013.03.001.

[30] K. Holmberg and A. Erdemir, “Influence of tribology on global energy consumption, costs and emissions,” *Friction 2017 5:3*, vol. 5, no. 3, pp. 263–284, Sep. 2017, doi: 10.1007/S40544-017-0183-5.

[31] B. Bhushan, “Modern Tribology Handbook, Two Volume Set,” *Modern Tribology Handbook, Two Volume Set*, Dec. 2000, doi: 10.1201/9780849377877/MODERN-TRIBOLOGY-HANDBOOK-TWO-VOLUME-SET-BHARAT-BHUSHAN.

[32] H. Beiβner and W. Schüler, “Dry lubricants for bobbinet machines,” DD 44117, Dec. 23, 1995

[33] S. H. Wu, “Use of Magnesium Stearate Dihydrate for Lubrication of Solid Industrial or Consumer Products,” US20100316585A1, Feb. 11, 2009 Accessed: Jan. 25, 2022. [Online]. Available: www.www.www.raw.u.uwww.my

[34] J. W. Purseglove, “Castor, Sesame & Safflower By E. A. Weiss London: Leonard Hill Books (1971), pp. 901, £16.00.,” *Experimental Agriculture*, vol. 8, no. 3, pp. 282–282, Jul. 1972, doi: 10.1017/S0014479700005366.

[35] E. Richard. Booser, American Society of Lubrication Engineers., and Society of Tribologists and Lubrication Engineers., “CRC handbook of lubrication : theory and practice of tribology,” CRC Press, 1983. Accessed: Jan. 25, 2022. [Online]. Available: https://www.routledge.com/CRC-Handbook-of-Lubrication-and-Tribology-Volume-III-Monitoring-Materials/Booser/p/book/9780849339035

[36] X. Zhang, J. Golding, and I. Burgar, “Thermal decomposition chemistry of starch studied by 13C high-resolution solid-state NMR spectroscopy,” *Polymer (Guildf)*, vol. 43, no. 22, pp. 5791–5796, Sep. 2002, doi: 10.1016/S0032-3861(02)00546-3.

[37] SUNDBERG JILL, “Triboactive Low-Friction Coatings Based on Sulfides and Carbides,” UPPSALA, 2014.

[38] C. P. Mulligan and D. Gall, “CrN–Ag self-lubricating hard coatings,” *Surface and Coatings Technology*, vol. 200, no. 5–6, pp. 1495–1500, Nov. 2005, doi: 10.1016/J.SURFCOAT.2005.08.063.

[39] H. A. Jehn, “Multicomponent and multiphase hard coatings for tribological applications,” *Surface and Coatings Technology*, vol. 131, no. 1–3, pp. 433–440, Sep. 2000, doi: 10.1016/S0257-8972(00)00783-0.

[40] A. Savan, E. Pflüger, R. Goller, and W. Gissler, “Use of nanoscaled multilayer and compound films to realize a soft lubrication phase within a hard, wear-resistant matrix,” *Surface and Coatings Technology*, vol. 126, no. 2–3, pp. 159–165, Apr. 2000, doi: 10.1016/S0257-8972(00)00542-9.

[41] A. A. Voevodin, J. P. O’Neill, and J. S. Zabinski, “WC/DLC/WS2 nanocomposite coatings for aerospace tribology,” *Tribology Letters 1999 6:2*, vol. 6, no. 2, pp. 75–78, 1999, doi: 10.1023/A:1019163707747.

[42] G. E. Totten, Ed., *Friction, Lubrication, and Wear Technology*. ASM International, 2017. doi: 10.31399/asm.hb.v18.9781627081924.

[43] A. Madhukar, “Structural classification of layered dichalcogenides of group IV B, V B and VI B transition metals,” *Solid State Communications*, vol. 16, no. 4, pp. 383–388, Feb. 1975, doi: 10.1016/0038-1098(75)90092-7.

[44] P. D. Fleischauer, “Fundamental aspects of the electronic structure, materials properties and lubrication performance of sputtered MoS2 films,” *Thin Solid Films*, vol. 154, no. 1–2, pp. 309–322, Nov. 1987, doi: 10.1016/0040-6090(87)90375-0.

[45] M. R. Vazirisereshk, A. Martini, D. A. Strubbe, and M. Z. Baykara, “Solid Lubrication with MoS2: A Review,” *Lubricants 2019, Vol. 7, Page 57*, vol. 7, no. 7, p. 57, Jul. 2019, doi: 10.3390/LUBRICANTS7070057.

[46] J. K. Lancaster, “A review of the influence of environmental humidity and water on friction, lubrication and wear,” *Tribology International*, vol. 23, no. 6, pp. 371–389, Dec. 1990, doi: 10.1016/0301-679X(90)90053-R.

[47] H. S. Khare and D. L. Burris, “The effects of environmental water and oxygen on the temperature-dependent friction of sputtered molybdenum disulfide,” *Tribology Letters*, vol. 52, no. 3, pp. 485–493, Dec. 2013, doi: 10.1007/S11249-013-0233-8.

[48] C. Donnet, J. M. Martin, T. le Mogne, and M. Belin, “Super-low friction of MoS2 coatings in various environments,” *Tribology International*, vol. 29, no. 2, pp. 123–128, Feb. 1996, doi: 10.1016/0301-679X(95)00094-K.

[49] K. Matsumoto and M. Suzuki, “Tribological Performance of Sputtered MoS 2 Films in Various Environment-influence of oxygen concentration, water vapor and gas species,” pp. 23–29, 2001, Accessed: Jan. 25, 2022. [Online]. Available: https://www.esmats.eu/esmatspapers/pastpapers/pdfs/1999/matsumoto.pdf

[50] J. L. Grosseau-Poussard, P. Moine, and M. Brendle, “Shear strength measurements of parallel MoSx thin films,” *Thin Solid Films*, vol. 307, no. 1–2, pp. 163–168, Oct. 1997, doi: 10.1016/S0040-6090(97)00205-8.

[51] R. Gilmore, M. A. Baker, P. N. Gibson, and W. Gissler, “Preparation and characterisation of low-friction TiB2-based coatings by incorporation of C or MoS2,” *SURFACE & COATINGS TECHNOLOGY*, vol. 105, no. 1–2, pp. 45–50, Jun. 1998, doi: 10.1016/S0257-8972(98)00445-9.

[52] R. Goller, P. Torri, M. A. Baker, R. Gilmore, and W. Gissler, “The deposition of low-friction TiN–MoSx hard coatings by a combined arc evaporation and magnetron sputter process,” *Surface & Coatings Technology*, vol. Complete, no. 120–121, pp. 453–457, 1999, doi: 10.1016/S0257-8972(99)00466-1.

[53] R. Gilmore *et al.*, “Low-friction TiN-MoS 2 coatings produced by dc magnetron co-deposition,” *Surface & Coatings Technology*, no. 108–109, pp. 345–351, 1998, Accessed: Jan. 25, 2022. [Online]. Available: https://www.infona.pl//resource/bwmeta1.element.elsevier-f8c19134-5cf3-32df-97ad-4129b78a77a2

[54] S. Carrera, O. Salas, J. J. Moore, A. Woolverton, and E. Sutter, “Performance of CrN/MoS 2 (Ti) coatings for high wear low friction applications,” *Surface & Coatings Technology*, vol. 1, no. 167, pp. 25–32, 2003, Accessed: Jan. 25, 2022. [Online]. Available: https://www.infona.pl//resource/bwmeta1.element.elsevier-4fde7ca5-43ab-35dd-97fc-d0783fdc5815

[55] J. S. Zabinski, M. S. Donley, and N. T. McDevitt, “Mechanistic study of the synergism between Sb2O3 and MoS2 lubricant systems using Raman spectroscopy,” *Wear*, vol. 165, no. 1, pp. 103–108, May 1993, doi: 10.1016/0043-1648(93)90378-Y.

[56] T. Polcar and A. Cavaleiro, “Review on self-lubricant transition metal dichalcogenide nanocomposite coatings alloyed with carbon,” *Surface and Coatings Technology*, vol. 206, no. 4, pp. 686–695, Nov. 2011, doi: 10.1016/J.SURFCOAT.2011.03.004.

[57] N. Onofrio, D. Guzman, and A. Strachan, “Novel doping alternatives for single-layer transition metal dichalcogenides,” *Journal of Applied Physics*, vol. 122, no. 18, p. 185102, Nov. 2017, doi: 10.1063/1.4994997.

[58] V. Buck, “Preparation and properties of different types of sputtered MoS2 films,” *Wear*, vol. 114, no. 3, pp. 263–274, Feb. 1987, doi: 10.1016/0043-1648(87)90116-5.

[59] V. Fox, J. Hampshire, and D. Teer, “MoS2/metal composite coatings deposited by closed-field unbalanced magnetron sputtering: tribological properties and industrial uses,” *Surface and Coatings Technology*, vol. 112, no. 1–3, pp. 118–122, Feb. 1999, doi: 10.1016/S0257-8972(98)00798-1.

[60] J. M. Martin, H. Pascal, C. Donnet, T. le Mogne, J. L. Loubet, and T. Epicier, “Superlubricity of MoS2: crystal orientation mechanisms,” *Surface and Coatings Technology*, vol. 68–69, no. C, pp. 427–432, Dec. 1994, doi: 10.1016/0257-8972(94)90197-X.

[61] C. Donnet, J. M. Martin, T. le Mogne, and M. Belin, “The origin of super-low friction coefficient of MoS2 coatings in various environments,” *Tribology Series*, vol. 27, no. C, pp. 277–284, Jan. 1994, doi: 10.1016/S0167-8922(08)70317-1.

[62] T. W. Scharf and S. v. Prasad, “Solid lubricants: a review,” *Journal of Materials Science 2012 48:2*, vol. 48, no. 2, pp. 511–531, Dec. 2012, doi: 10.1007/S10853-012-7038-2.

[63] The Editors of Encyclopaedia, Ed., “nitrile rubber ,” *Britannica*, vol. 4. 2016. Accessed: Jan. 25, 2022. [Online]. Available: https://www.britannica.com/technology/nitrile-rubber

[64] “NBR.” https://polymerdatabase.com/Elastomers/NBR.html (accessed Jan. 25, 2022).

[65] G. Schmid, “Nanostructured Surfaces,” in *Nanotechnology*, vol. 8, Wiley-VCH, 2010. Accessed: Jan. 25, 2022. [Online]. Available: https://www.wiley.com/en-us/Nanotechnology%3A+Volume+8%3A+Nanostructured+Surfaces-p-9783527317394

[66] G. K. Wehner, “Sputtering of Metal Single Crystals by Ion Bombardment,” *Journal of Applied Physics*, vol. 26, no. 8, pp. 239–298, May 2004, doi: 10.1063/1.1722136.

[67] E. Kay, “Impact Evaporation and Thin Film Growth in a Glow Discharge,” *Advances in Electronics and Electron Physics*, vol. 17, no. C, pp. 245–322, Jan. 1963, doi: 10.1016/S0065-2539(08)60027-X.

[68] M. Ohring, “Deposition and structure,” in *Material Science of Thin Films*, 2nd ed., Academic Press, 2001. Accessed: Jan. 25, 2022. [Online]. Available: https://books.google.es/books?hl=es&lr=&id=m3fai5hbc94C&oi=fnd&pg=PP1&dq=Ohring+M+(2002)+Material+science+of+thin+films,+deposition+and+structure,+2nd+edn.+Academic&ots=S2a4f8qiTx&sig=XQoW0S7M2Me8w2iX-gfMTnk3jBI#v=onepage&q&f=false

[69] K. v Gadepally and R. M. Hawk, “Integrated Circuits Interconnect Metallization for the Submicron Age,” *J Ark Acad Sci*, vol. 43, no. 9, 1989, Accessed: Jan. 25, 2022. [Online]. Available: http://scholarworks.uark.edu/jaashttp://scholarworks.uark.edu/jaas/vol43/iss1/9

[70] M. M. Hassan, “Antimicrobial Coatings for Textiles,” in *Handbook of Antimicrobial Coatings*, Elsevier, 2018, pp. 321–355. doi: 10.1016/B978-0-12-811982-2.00016-0.

[71] I. V. Tudose *et al.*, “Chemical and physical methods for multifunctional nanostructured interface fabrication,” in *Functional Nanostructured Interfaces for Environmental and Biomedical Applications*, Elsevier, 2019, pp. 15–26. doi: 10.1016/B978-0-12-814401-5.00002-5.

[72] J. Wang *et al.*, “Magnetron-sputtering deposited $WTe_2$for an ultrafast thulium-doped fiber laser,” *Optics Letters, Vol. 42, Issue 23, pp. 5010-5013*, vol. 42, no. 23, pp. 5010–5013, Dec. 2017, doi: 10.1364/OL.42.005010.

[73] T. Vuchkov, M. Evaristo, T. bin Yaqub, and A. Cavaleiro, “The effect of substrate location on the composition, microstructure and mechano-tribological properties of W-S-C coatings deposited by magnetron sputtering,” *Surface and Coatings Technology*, vol. 386, Mar. 2020, doi: 10.1016/J.SURFCOAT.2020.125481.

[74] B. Window and N. Savvides, “Charged particle fluxes from planar magnetron sputtering sources,” *Journal of Vacuum Science & Technology A: Vacuum, Surfaces, and Films*, vol. 4, no. 2, p. 196, Jun. 1998, doi: 10.1116/1.573470.

[75] J. T. Gudmundsson and D. Lundin, “Introduction to magnetron sputtering,” *High Power Impulse Magnetron Sputtering: Fundamentals, Technologies, Challenges and Applications*, pp. 1–48, Jan. 2020, doi: 10.1016/B978-0-12-812454-3.00006-1.

[76] A. A. Voevodin, J. P. O’Neill, and J. S. Zabinski, “Nanocomposite tribological coatings for aerospace applications,” *Surface and Coatings Technology*, vol. 116–119, pp. 36–45, Sep. 1999, doi: 10.1016/S0257-8972(99)00228-5.

[77] T. Polcar and A. Cavaleiro, “Self-adaptive low friction coatings based on transition metal dichalcogenides,” *Thin Solid Films*, vol. 519, no. 12, pp. 4037–4044, Apr. 2011, doi: 10.1016/J.TSF.2011.01.180.

[78] T. Polcar, M. Evaristo, M. Stueber, and A. Cavaleiro, “Mechanical and tribological properties of sputtered Mo–Se–C coatings,” *Wear*, vol. 266, no. 3–4, pp. 393–397, Feb. 2009, doi: 10.1016/J.WEAR.2008.04.010.

[79] M. Evaristo, T. Polcar, and A. Cavaleiro, “Can WÀSeÀC Coatings Be Competitive to WÀSÀC Ones?”, doi: 10.1002/ppap.200930414.

[80] T. Vuchkov, M. Evaristo, T. bin Yaqub, T. Polcar, and A. Cavaleiro, “Synthesis, microstructure and mechanical properties of W–S–C self-lubricant thin films deposited by magnetron sputtering,” *Tribology International*, vol. 150, p. 106363, Oct. 2020, doi: 10.1016/J.TRIBOINT.2020.106363.

[81] J. Caessa, T. Vuchkov, T. bin Yaqub, and A. Cavaleiro, “On the Microstructural, Mechanical and Tribological Properties of Mo-Se-C Coatings and Their Potential for Friction Reduction against Rubber,” *Materials 2021, Vol. 14, Page 1336*, vol. 14, no. 6, p. 1336, Mar. 2021, doi: 10.3390/MA14061336.

[82] T. Vuchkov, T. bin Yaqub, M. Evaristo, and A. Cavaleiro, “Synthesis, microstructural and mechanical properties of self-lubricating Mo-Se-C coatings deposited by closed-field unbalanced magnetron sputtering,” *Surface and Coatings Technology*, vol. 394, p. 125889, Jul. 2020, doi: 10.1016/J.SURFCOAT.2020.125889.

[83] “Standard Test Method for Adhesion Strength and Mechanical Failure Modes of Ceramic Coatings by Quantitative Single Point Scratch Testing.” https://www.astm.org/c1624-22.html (accessed May 30, 2022).

[84] W. C. Oliver and G. M. Pharr, “An improved technique for determining hardness and elastic modulus using load and displacement sensing indentation experiments,” *Journal of Materials Research 1992 7:6*, vol. 7, no. 6, pp. 1564–1583, Jan. 2011, doi: 10.1557/JMR.1992.1564.

[85] D. Nečas and P. Klapetek, “Gwyddion: An open-source software for SPM data analysis,” *Central European Journal of Physics*, vol. 10, no. 1, pp. 181–188, Feb. 2012, doi: 10.2478/S11534-011-0096-2/MACHINEREADABLECITATION/RIS.

[86] “OriginLab - Origin and OriginPro - Data Analysis and Graphing Software.” https://www.originlab.com/ (accessed May 30, 2022).

[87] “H11 Tool Steel AISI | 1.2343 | X37CrMoV5-1 | SKD6 | BH11 - Otai Special Steel.” https://www.astmsteel.com/product/h11-tool-steel/ (accessed May 13, 2022).

[88] J. Sundberg, “Triboactive Low-Friction Coatings Based on Sulfides and Carbides,” Uppsala University, Uppsala, 2014. doi: 10.1016/J.APSUSC.2014.03.038.

[89] T. Vuchkov, T. bin Yaqub, M. Evaristo, and A. Cavaleiro, “Synthesis, microstructural and mechanical properties of self-lubricating Mo-Se-C coatings deposited by closed-field unbalanced magnetron sputtering,” *Surface and Coatings Technology*, vol. 394, p. 125889, Jul. 2020, doi: 10.1016/J.SURFCOAT.2020.125889.

[90] J. C. Bernède, “About the preferential sputtering of chalcogen from transition metal dichalcogenide compounds and the determination of compound stoichiometry from XPS peak positions,” *Applied Surface Science*, vol. 171, no. 1–2, pp. 15–20, Feb. 2001, doi: 10.1016/S0169-4332(00)00535-3.

[91] J. R. Lince, M. R. Hilton, and A. S. Bommannavar, “Oxygen substitution in sputter-deposited MoS2 films studied by extended X-ray absorption fine structure, X-ray photoelectron spectroscopy and X-ray diffraction,” *Surface and Coatings Technology*, vol. 43–44, no. PART 2, pp. 640–651, Dec. 1990, doi: 10.1016/0257-8972(90)90008-Z.

[92] T. Polcar, M. Evaristo, M. Stueber, and A. Cavaleiro, “Synthesis and structural properties of Mo–Se–C sputtered coatings,” *Surface and Coatings Technology*, vol. 202, no. 11, pp. 2418–2422, Feb. 2008, doi: 10.1016/J.SURFCOAT.2007.08.019.

[93] A. v. Bondarev, P. v. Kiryukhantsev-Korneev, A. N. Sheveyko, and D. v. Shtansky, “Structure, tribological and electrochemical properties of low friction TiAlSiCN/MoSeC coatings,” *Applied Surface Science*, vol. 327, pp. 253–261, Feb. 2015, doi: 10.1016/J.APSUSC.2014.11.150.

[94] I. Ahmad *et al.*, “Influence of strain on specific features of MoX2 (X = S, Se, Te) monolayers,” *Physica B: Condensed Matter*, vol. 545, pp. 113–118, Sep. 2018, doi: 10.1016/J.PHYSB.2018.05.034.

[95] S. Sharma, “TRIBOLOGICAL BEHAVIOUR OF LASER TREATED C-ALLOYED TMD COATINGS IN RUBBER CONTACT ”.

[96] T. Polcar, M. Evaristo, and A. Cavaleiro, “The tribological behavior of W–S–C films in pin-on-disk testing at elevated temperature,” *Vacuum*, vol. 81, no. 11–12, pp. 1439–1442, Aug. 2007, doi: 10.1016/J.VACUUM.2007.04.010.

[97] J. Musil, F. Kunc, H. Zeman, and H. Poláková, “Relationships between hardness, Young’s modulus and elastic recovery in hard nanocomposite coatings,” *Surface and Coatings Technology*, vol. 154, no. 2–3, pp. 304–313, May 2002, doi: 10.1016/S0257-8972(01)01714-5.

[98] A. Leyland and A. Matthews, “On the significance of the H/E ratio in wear control: a nanocomposite coating approach to optimised tribological behaviour,” *Wear*, vol. 246, no. 1–2, pp. 1–11, Nov. 2000, doi: 10.1016/S0043-1648(00)00488-9.

[99] P. Nicolini, R. Capozza, P. Restuccia, and T. Polcar, “Structural Ordering of Molybdenum Disulfide Studied via Reactive Molecular Dynamics Simulations,” *ACS Applied Materials and Interfaces*, vol. 10, no. 10, pp. 8937–8946, Mar. 2018, doi: 10.1021/ACSAMI.7B17960/SUPPL_FILE/AM7B17960_SI_001.PDF.

[100] W. Liu, Y. Zheng, T. Wang, L. Lv, and Z. Yang, “A study on testing of rubber friction coefficient and its wear surface by UMT-2,” *IOP Conference Series: Materials Science and Engineering*, vol. 772, no. 1, Mar. 2020, doi: 10.1088/1757-899X/772/1/012052.

[101] J. M. Martin, “Superlubricity of Molybdenum Disulfide,” *Superlubricity*, pp. 207–225, Jan. 2007, doi: 10.1016/B978-044452772-1/50044-5.

[102] C. L. Dong, C. Q. Yuan, X. Q. Bai, X. P. Yan, and Z. Peng, “Tribological properties of aged nitrile butadiene rubber under dry sliding conditions,” *Wear*, vol. 322–323, pp. 226–237, Jan. 2015, doi: 10.1016/J.WEAR.2014.11.010.